REVIEW

Check for updates

Recent advances in nanoprecipitation: from mechanistic insights to applications in nanomaterial synthesis

Muzammil Kuddushi, [ID] [a] Chiranjeevi Kanike, [ID] [a] Ben Bin Xu [ID] *[b] and Xuehua Zhang [ID] *[a]

Nanoprecipitation is a versatile, low-energy technique for synthesizing nanomaterials through controlled precipitation, enabling precise tuning of material properties. This review offers a comprehensive and up-to-date perspective on nanoprecipitation, focusing on its role in nanoparticle synthesis and its adaptability in designing diverse nanostructures. The review begins with the foundational principles of nanoprecipitation, emphasizing the impact of key parameters such as flow rate, mixing approach, injection rate, and Reynolds number on nanomaterial characteristics. It also discusses the influence of physicochemical factors, including solvent choice, polymer type, and drug properties. Various nano-precipitation configurations—batch, flash, and microfluidic are examined for their specific advantages in controlling particle size, morphology, and internal structure. The review further explores the potential of nanoprecipitation to create complex nanostructures, such as core–shell particles, Janus nanoparticles, and porous and semiconducting polymer nanoparticles. Applications in biomedicine and other fields highlight nanoprecipitation's promise as a sustainable and tunable method for fabricating advanced nanomaterials. Finally, the review identifies future directions, including scaling microfluidic techniques, expanding compatibility with hydrophilic compounds, and integrating machine learning to further enhance the development of nanoprecipitation.

Introduction

Nanoprecipitation, a simple solution-based approach for the preparation of nanoparticles, was first introduced by Fessi *et al.*[1,2] Recently, it has gained increasing attention as a versatile technique for the synthesis of novel nanomaterials, owing to its simplicity, low energy requirements, ease of implementation, tunability, reproducibility, and versatility. Nanomaterials produced *via* nanoprecipitation include polymer particles,[3–6] cellulose acetate particles,[7] protein nanoparticles,[8] semiconductor nanoparticles,[9,10] Janus nanoparticles,[11,12] nanocrystals,[13] and mesoporous particles.[14] One significant advantage of nanoprecipitation is its ability to form nanoparticles without requiring surfactants or toxic, undesirable organic solvents during synthesis. Recent advancements in nanoprecipitation techniques have further enhanced its efficiency, enabling the development of new functional nanomaterials.

A typical nanoprecipitation process involves mixing a polymer solution dissolved in an organic solvent with an aqueous solution. When the organic solution containing polymers rapidly and uniformly mixes with the aqueous non-solvent, it crosses the solubility barrier, resulting in the precipitation or phase separation of the solute into nanoparticles within the continuous phase. The resulting oversaturation and chain collapse lead to the formation of polymer nanoparticles (PNPs), which can range in size from a few nanometers to several micrometers. The formation of these nanomaterials involves three key processes: (1) mixing of the organic solution (containing solute molecules) with an anti-solvent (aqueous phase), (2) nucleation of solute molecules, and (3) aggregation and growth into nanomaterials.[7,15–17] This same process can also nucleate liquid droplets through spontaneous emulsification, a phenomenon known as the "ouzo effect" or solvent exchange in flow systems.[18–21] Alternatively, similar effects can occur in evaporating ternary liquid mixtures.[22,23]

Several review articles have summarized specific aspects of preparing polymer nanoparticles (PNPs).[24–27] In this review, we aim to provide an updated and holistic perspective on the physicochemical aspects and hydrodynamics that significantly influence nanoprecipitation. We place particular emphasis on

[a] Department of Chemical and Materials Engineering, University of Alberta, Alberta T6G 1H9, Canada. E-mail: xuehua.zhang@ualberta.ca

[b] Mechanical and Construction Engineering, Faculty of Engineering and Environment, Northumbria University, Newcastle Upon Tyne NE1 8ST, UK. E-mail: ben.xu@northumbria.ac.uk

the solution and flow conditions in various mixing configurations used during synthesis and their impact on controlling nanomaterial formation. Additionally, we discuss the fundamental principles of different mixing configurations for nanoprecipitation. Special attention is given to key parameters, such as mixing methods and conditions, including flow rate, stream velocity, injection rate, and the properties of fluids and their compositions – such as solvent, non-solvent, polymer, and the physicochemical conditions of the liquid mixtures.[28] The general principles discussed in this review provide a framework for understanding how the final size, structure, and properties of nanomaterials are determined. While the field of nanoprecipitation is rapidly evolving, and it is beyond the scope of this review to cover all recent articles, we aim to present representative examples in each section. These examples are intended to inspire further exploration and advancements in future studies.

Basic principles of nanoprecipitation

The nanoprecipitation technique relies on the transition from miscibility to immiscibility, achieved by mixing an organic solution of the solute (*e.g.*, polymers or small molecules) with an anti-solvent (miscible with the organic phase but a non-solvent for the solute), as illustrated in Fig. 1(a). Nanoparticle formation occurs by reducing the solvent quality through the addition of the anti-solvent. This technique is also known as
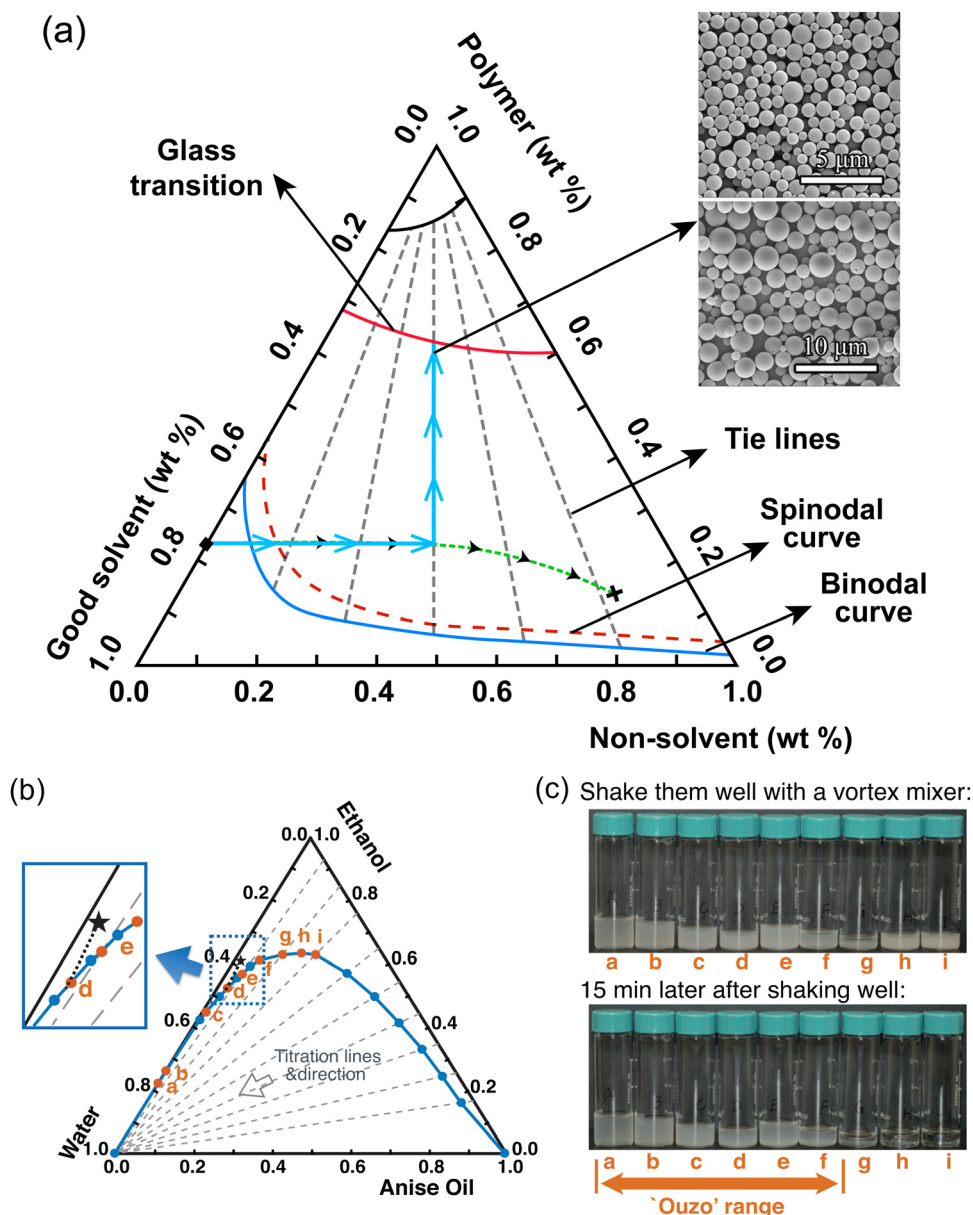

Fig. 1 Nanoprecipitation in ternary systems. (a) Ternary phase diagram for a polymer in a binary solvent and the SEM images of the synthesized polymer nanoparticle.[15,32] (b) Solubility diagram and (c) photos of the ternary mixtures of ethanol, water, and anise oil.[22]

solvent shifting, solvent displacement, anti-solvent precipitation, or solvent exchange, the latter referring to the anti-solvent displacing the solution in a directional flow.[19,29,30] When the organic and aqueous phases are mixed, the process leads to rapid saturation of the solute to its critical nucleation concentration. This occurs due to the miscibility between the solvent and anti-solvent, combined with the solute's immiscibility in the anti-solvent. Fig. 1(b) shows the ternary diagram of water, ethanol, and anise oil, with the blue solid line representing the measured phase-separation curve. The black star and the black dotted line in the inset indicate the initial composition of the Ouzo drop and its trajectory over time-based on numerical simulations. The gray dashed lines represent the paths of various composition coordinates from titration experiments. Fig. 1(c) shows the stability of the macrosuspension for compositions labeled (a)–(i) in the ternary diagram. This comparison reveals that the curve connecting the solid circles (a)–(f) in Fig. 1(b) marks the boundary of the Ouzo region, corresponding to the critical composition at which the Ouzo effect occurs. The process of nanoparticle formation can be understood through thermodynamic principles. As the solvent quality decreases, the solute experiences a supersaturation state, driving nucleation. According to classical nucleation theory, the critical nucleus size is determined by the balance of volumetric free energy change and interfacial energy. High supersaturation lowers the energy barrier for nucleation, promoting the rapid formation of numerous small particles.[31]

Many ternary mixtures consist of both miscible pairs and immiscible pairs. The solutes in such systems can include polymers, oils,[33–36] or even gases.[37,38] When the solute is oil, the nanoprecipitation process is equivalent to what is commonly referred to as the Ouzo effect.[22,23,29] The most common solvent and anti-solvent combinations for nanoprecipitation are polar organic solvents with water (or an aqueous solution). However, other combinations are also feasible, including organic solvent–organic solvent systems,[34–36] ionic liquid–ionic liquid systems,[39,40] and deep eutectic solvents.[41]

The nucleation and growth of supersaturated solute molecules lead to the formation of polymer nanoparticles. Once nucleation is initiated, the growth of nanoparticles proceeds *via* the diffusion of solute molecules from the surrounding medium. Fick's laws of diffusion describe the transport of solute molecules, where the flux is proportional to the concentration gradient. Fast diffusion ensures uniform particle growth, while variations in local concentrations can lead to particle size heterogeneity. Both kinetic and thermodynamic factors play a role in the particle structure and size distribution.[6,42–44] Both mixing and diffusion processes occur simultaneously, depleting the solute molecules in the mixture. Additionally, the anti-solvent dilutes the solute, reducing its concentration. As the solute concentration falls below the critical nucleation threshold, nucleation and growth cease. The formed nanoparticles remain dispersed in the mixture, trapped in a thermodynamically metastable state. The rate of oversaturation plays a critical role in determining nanoparticle size. A high nucleation rate leads to the formation of smaller particles with a narrow size distribution. A key complexity in this process is that nanoparticle formation arises from local and temporal oversaturation of the solute during mixing. Oversaturation evolves over time and may also vary spatially. Both the physicochemical properties of the compounds in the mixture and the mixing dynamics between the solution and the antisolvent are critical in creating the out-of-equilibrium oversaturation, which determines the size, structure, and properties of the nanoparticles. Interfacial tension plays a crucial role in the stabilization of nanoparticles. The presence of stabilizers or surfactants reduces interfacial energy, preventing coalescence.

Mixing processes in nanoprecipitation

The properties of synthesized nanoparticles depend on various factors, including mixing conditions, solvent composition, stabilizing agents, and physicochemical parameters.[16,45] Efficient mixing is critical for achieving uniform particle size and morphology. The hydrodynamic flow regime, characterized by the Reynolds number (Re), governs the mixing dynamics. Laminar flow (Re < 2100) provides controlled mixing suitable for precision nanoprecipitation, while turbulent flow (Re > 4000) improves mixing rates but may introduce shear stress, affecting particle stability. Additionally, the Damköhler number (Da), which compares the timescales of reaction and mixing, is crucial in determining the uniformity of the synthesized nanoparticles. When (Da < 1), mixing dominates, ensuring homogeneity, whereas (Da > 1) can result in heterogeneities due to reaction dominance.[46]

There are three primary nanoprecipitation techniques: batch, flash, and microfluidic methods, as illustrated in Fig. 2. In batch nanoprecipitation (BNP), the polymer solution and solvent are mixed rapidly, either through dropwise addition[47] or by injecting the entire polymer solution directly into the aqueous medium, as shown in Fig. 2(a).[48] In batch processes, the degree of mixing significantly influences the oversaturation dynamics. Rapid mixing reduces local concentration gradients, promoting uniform nucleation and growth. The shear forces generated during mixing also play a pivotal role, as they impact the particle size distribution and morphology. Controlled addition can also be achieved using a syringe pump or slow diffusion across a dialysis membrane. Several factors—such as the mixing method,[49] the polymer's molecular weight,[50] and the choice of organic solvent[45]—influence the size and morphology of polymer nanoparticles (PNPs) synthesized *via* BNP. Perevyazko *et al.* demonstrated the fabrication of nanoparticles from solutions of poly(methyl methacrylate) and its copolymers. The particle characteristics strongly depended on the polymer's chemical structure and preparation method. In the studied cases, particle sizes ranged from 6–680 nm, with polydispersity indices (dw/dn) varying between 1.02 and 1.40. Their findings showed that nanoparticles of a desirable size range could be synthesized using solvent–nonsolvent methods. Fig. 3(a)–(f) shows the formation of nanoparticles by the batch process, achieved by varying the acetone-to-water solvent ratio.
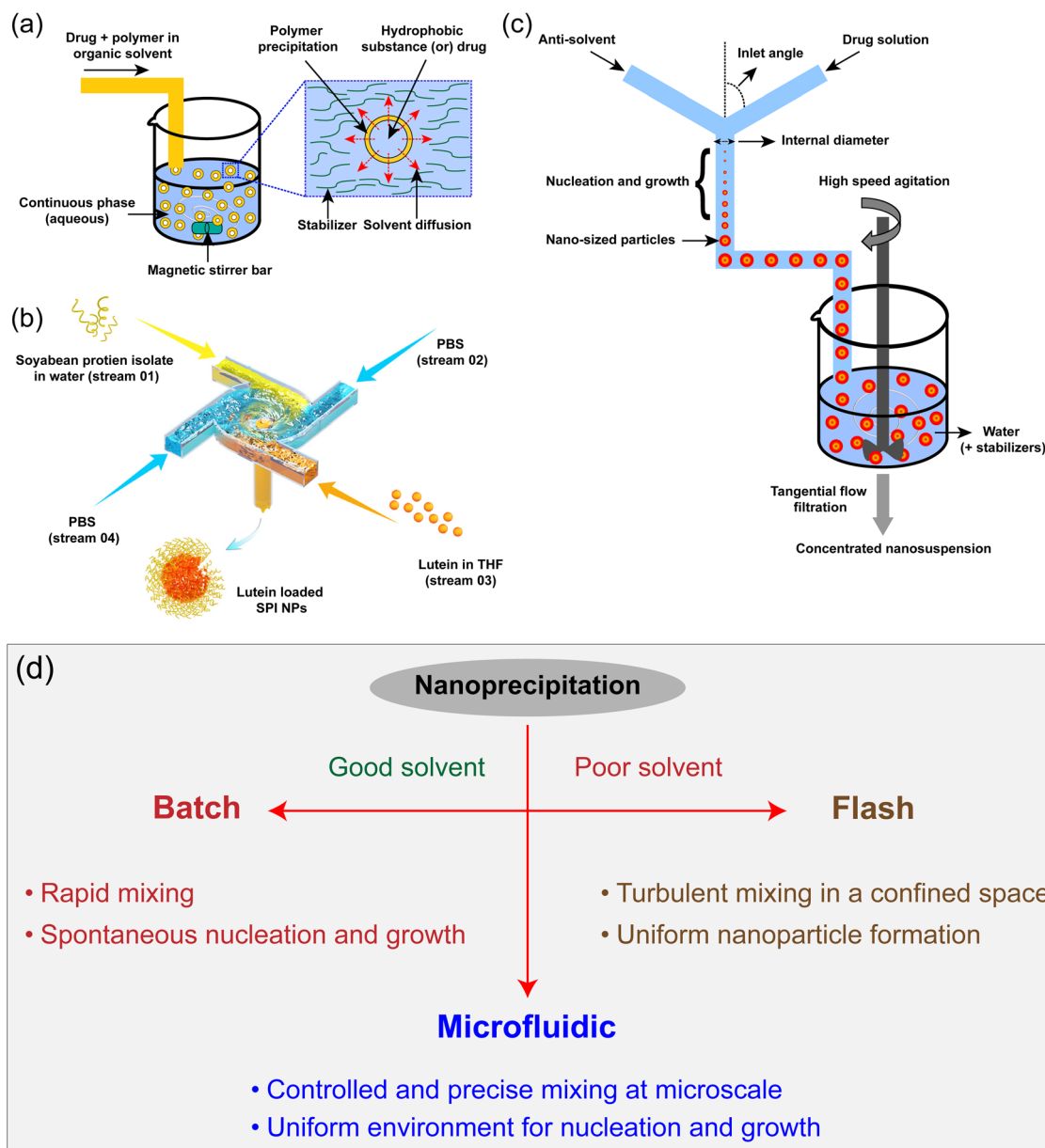
Fig. 2 Major types of mixing processes for nanoprecipitation. (a) Batch nanoprecipitation (BNP),[48] (b) flash nanoprecipitation (FNP),[51] and (c) microfluidic nanoprecipitation (MNP),[52] (d) principles of batch, flash, and microfluidic nanoprecipitation techniques.

Flash nanoprecipitation (FNP) utilizes a high-pressure injection pump to rapidly mix streams of organic solution and nonsolvent within a confined chamber, typically for milliseconds. The high shear forces generated during FNP facilitate rapid diffusion and mixing at the molecular level. The confinement within a narrow chamber ensures consistent mixing, minimizing spatial concentration gradients. The interplay between shear rates and mixing efficiency directly impacts particle size and uniformity, with higher shear rates promoting smaller, more homogeneous particles. This promotes the rapid formation of polymer colloids with specific morphologies and compositions.[17,51,54,55] Wang *et al.* fabricated lutein-loaded nanoparticles (NPs) using FNP. In their process (Fig. 2(b)),

SPI was dissolved in water at a fixed concentration of 0.8 mg mL^{-1}, which represents the maximum solubility of SPI under the designed conditions. The properties of the kinetically controlled SPI NPs, including particle size, size distribution, drug loading efficiency, stability, and bioavailability, were investigated as well.[51]

Microfluidic nanoprecipitation (MNP) has been described as a simple method for drug nanosizing.[56,57] Microfluidic systems rely on precise control of flow dynamics, which are dictated by the dimensions and geometry of the channels. The mixing efficiency in microfluidics is enhanced by chaotic advection and rapid diffusion-driven processes. By adjusting flow rates and channel configurations, it is possible to achieve highly
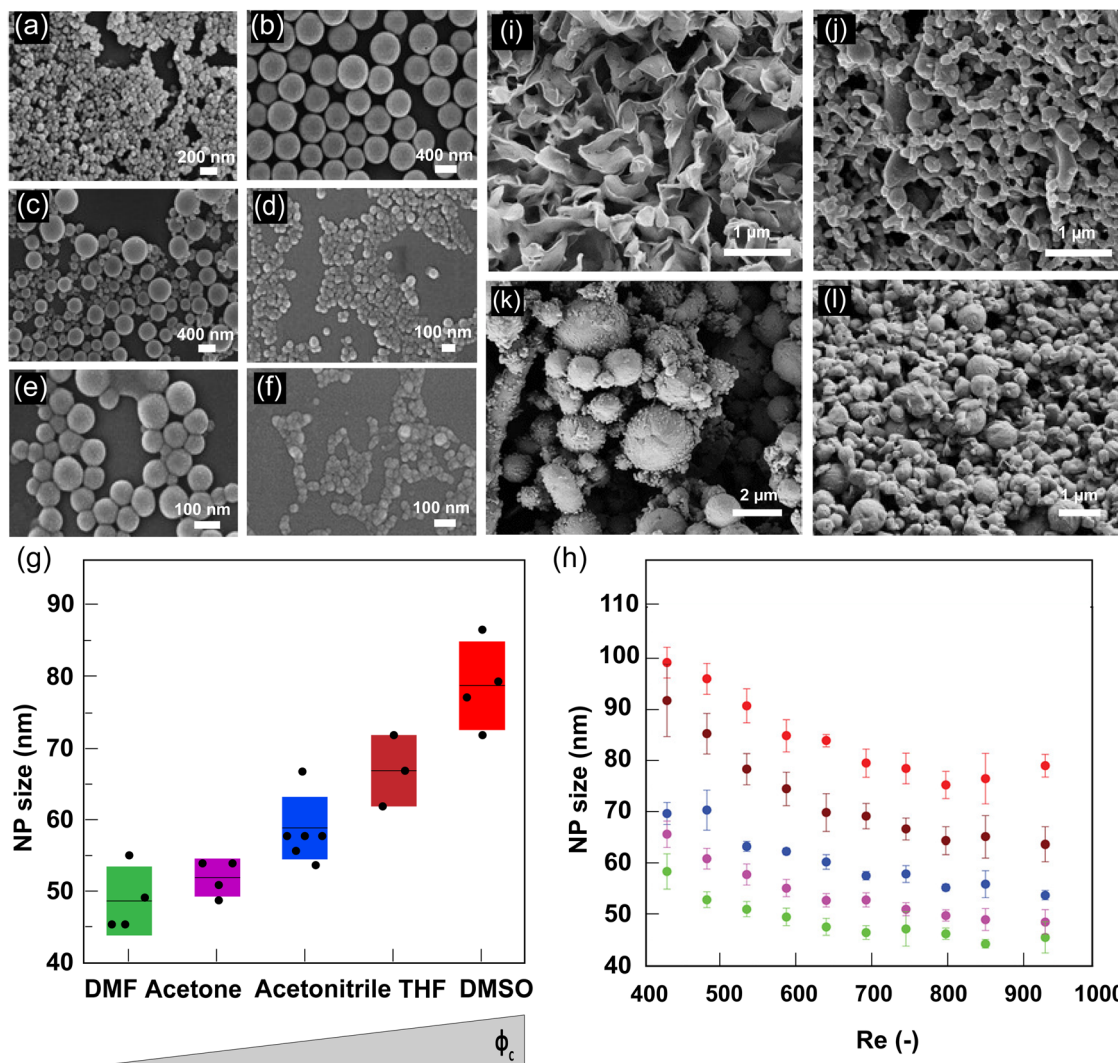
Fig. 3 Polymer nanoparticles (PNPs) prepared by nanoprecipitation. (a)–(f) SEM image of the PNPs prepared using two polymer poly(MMA-*stat*-pyMAA) (PMMA) and copolymer poly(MMA-*stat*-EA). (a)–(c) PMMA; (d)–(f) PMMA and copolymer. The mixing conditions are by dripping acetone to water (a) and (d), by dialysis of *N*,*N*-dimethylacetamide (c) and (f), or by dripping water to acetone (b) and (e).[49] Variation of the PNP size as a function of (a) solvents under constant mixing kinetics (Re = 749), and (b) Reynolds number (Re = 400–1000).[45] (i)–(l) Field emission scanning electron microscopic image representing the variation of PNP size on the final polymer concentrations (i) 0 mg mL^{-1}, (j) 1 mg mL^{-1}, (k) 2 mg mL^{-1}, and (l) 5 mg mL^{-1} from an initial polymer concentration of 5 mg mL^{-1}.[53]

controlled nanoprecipitation, with particle sizes being inversely proportional to the flow rate due to enhanced nucleation at higher mixing velocities.[58] The results show that stable aqueous hydrocortisone NPs can be obtained using a bottom-up approach with microfluidic reactors. Particle size can be controlled by modifying the processing conditions and the design of the microfluidic reactors, such as internal diameters and inlet angles. Changes in flow rates were found to have a dominant effect on the size of the generated particles.[44,59] The setup typically includes a central channel squeezed by two vertical channels, which allows for rapid diffusion-driven mixing (Fig. 2(c)).[52] The dimensions of the channel, such as length, height, and structure, are key determinants of the properties of the particles in the microfluidic process.[56,60,61]

Slater *et al.* reported the preparation of hydrophobic branched NPs *via* rapid nanoprecipitation. The resulting aqueous nanoparticle dispersions were robust and stable to dilution, solvent addition, sonication, and temperature changes. The addition of small amounts of NaCl led to nanoparticle destabilization, suggesting that electrostatic repulsion is a key factor in maintaining stability. The presence of NaCl likely screens surface charges, reducing repulsive interactions and promoting aggregation, thereby emphasizing the role of charge stabilization.[62] Variation in particle size and fluorescent intensity at different H_2O/THF ratios (Fig. 4(i) and (j)) for EDP NPs ranged from 28 nm to 55 nm, while BDP NPs ranged from 20 nm to 80 nm (Fig. 4(k) and (l)). In the following sections, we will discuss FNP and MNP in more detail.
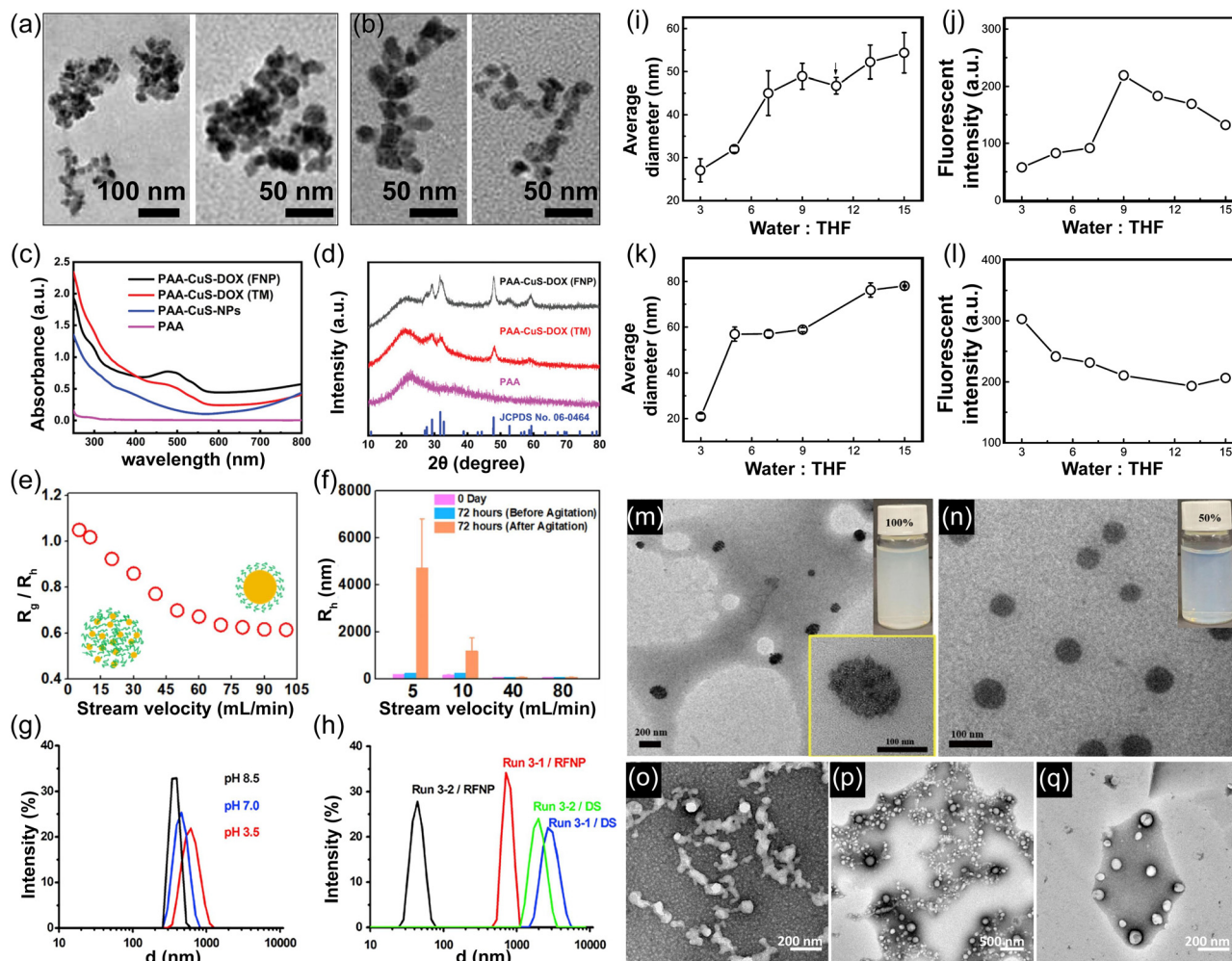
Fig. 4 TEM images of CuS-NPs-FNP with different AA/Cu ratios and corresponding hydrodynamic diameters of PAA-CuS-DOX NPs: (a) 1 (173 nm) and 2.5 (117 nm), (b) 5 (85 nm) and 20 (50 nm). Variation of hydrodynamic size distributions of CuS-NPs prepared *via* FNP and thermal method (TM) method (c) UV-vis spectra of NPs with and without drug (DOX) molecules prepared *via* FNP and TM. (d) XRD patterns of the NPs prepared *via* different FNP and TM methods with and without DOX molecules.[63] (e) The ratio of the radius of gyration to the hydrodynamic radius (R_g/R_h) of the PNPs at stream velocities. (f) Stability of the prepared PNPs as a function of time.[8] (g) and (h) Variation of PNP sizes at different solution pH.[64] RFNP: reactive nanoprecipitation. Run 3-1: without chitosan; run 3-2: with chitosan. DS: drip and stir method, in contrast to nanoprecipitation. (i)–(k) Variation of particle size and fluorescent intensity at different H_2O/THF ratio (i) and (j) for EDP NPs (k) and (l) BDP NPs.[65] (m) and (n) TEM images and the corresponding nanopesticide dispersion prepared using sophorolipids of mass concentrations (m) 100% acidic sophorolipids, and (n) 50% acidic sophorolipids and 50% lactonic sophorolipids.[66] (o)–(q) TEM images of the PNPs obtained using block copolymers of different molecular weights.[67]

Flash nanoprecipitation

Flash nanoprecipitation (FNP) enables the rapid, continuous production of polymer nanoparticles (PNPs) with smaller and more uniform particle sizes compared to batch nanoprecipitation (BNP).[68,69] Both flow conditions and material properties jointly influence the size, morphology, and loading efficiency of PNPs, underscoring the importance of parameter control for precise nanoparticle synthesis.[51,70]

Flow dynamics and mixing conditions, such as stream velocity, Reynolds number, and injection rate, are crucial in achieving desired particle characteristics. Wang *et al.* showed that increasing the Reynolds number over 1400 reduced the hydrodynamic size of PNPs from 122 nm to 80 nm, with minimal size change beyond this threshold.[51] Conversely, Zhao *et al.*

observed that higher flow rates in a buffer solution gradually increased particle size, with a significant size jump at very high flow rates, demonstrating the need for careful control over flow to maintain size uniformity.[71] Bhutto *et al.* investigated the internal structure of β-carotene-loaded protein PNPs, showing that increasing stream velocity resulted in densely packed core–shell structures, transitioning from laminar to turbulent flow. As stream velocity further increased, particle size stabilized, highlighting how flow dynamics affect internal particle organization and density, as shown in Fig. 4(e) and (f).[8]

Material properties, such as surfactant composition and polymer characteristics, also influence particle formation in FNP. Ma *et al.* examined the effect of surfactant ratio on lambda-cyhalothrin-loaded nanopesticides, finding that acidic

sophorolipids alone produced spindle-like particles while adding lactonic sophorolipids led to spherical particles due to altered hydrophobic interactions. This demonstrates how specific surfactant compositions can direct particle shape and stability (Fig. 4(m) and (n)[66]). Jia et al. used FNP to create stable, low-toxicity copper sulfate nanoparticles for chemotherapy. They observed that as stream velocity increased from 6 to 30 mL min^{-1}, particle size decreased from 64 nm to 50 nm, stabilizing beyond that point. Additionally, Jia et al.[63] demonstrated the effect of varying the AA/CuS ratio, as shown in Fig. 4(a) and (b), where increasing the ratio from 1 (173 nm) and 2.5 (117 nm) in Fig. 4(a) to 5 (85 nm) and 20 (50 nm) in Fig. 4(b) led to a significant reduction in particle size. This is due to PAA acting as a capping agent, inhibiting growth through steric hindrance and electrostatic stabilization. At lower ratios, limited PAA results in larger nanoparticles, while higher concentrations restrict growth, leading to smaller sizes. Beyond an AA/CuS ratio of 10, the particle size remains unchanged, indicating surface saturation with PAA. In Fig. 4(c) and (d), Jia et al.[63] demonstrated the successful loading of DOX into the PAA-CuS-DOX NPs, as confirmed by the absorbance peak at 500 nm in the UV-vis spectra, corresponding to the characteristic peak of DOX. XRD analysis was also performed to characterize the crystal structure of the PAA-CuS-DOX NPs. Despite the large background signal from the amorphous PAA polymer, intense characteristic crystalline CuS peaks were clearly observed, confirming the presence of the CuS crystal structure.

Zhu et al. reported the production of lead(II) sulfate (PbSO$_4$) nanosuspension, with an average particle diameter of ~50 nm, via in situ reactive flash nanoprecipitation. Fig. 4(h) shows chitosan as a pH-sensitive surface stabilizer whose hydrophobicity can be tuned by varying its pH (Fig. 4(g) and (h)). By increasing the pH of the suspension, the chitosan/PbSO$_4$ nanoparticles rapidly aggregated and settled down. After filtration and drying, the particles were easily separated from water, with significantly reduced size enlargement due to Ostwald ripening and recrystallization.[64] Pustulka et al.[67] present TEM images in Fig. 4, depicting (o) 5k–5k PEG-b-PLA, (p) 5k–10k PEG-b-PLGA, and (q) 10k–10k PEG-b-PLGA nanoparticles, which demonstrated stability in suspension for at least 10 days.

The influence of drug loading on particle properties has been explored in several studies. Zhao et al. used an FNP setup with a multi-inlet vortex mixer to prepare curcumin-loaded zein nanoparticles, finding that higher drug concentrations initially increased particle size and yield, with particles exhibiting narrow size distribution at higher drug levels.[71] Wang et al. similarly found that at low drug-to-polymer ratios, particle size initially decreased before increasing at higher ratios, indicating an optimal ratio range for controlling particle dimensions in drug-loaded systems.[51]

Nanoprecipitation in microfluidics

Microfluidic nanoprecipitation (MNP) allows precise control over polymer nanoparticle characteristics, including size, morphology, and surface properties.[61,72] The microfluidic setup uses ultra-low volumes (pico- to nanoliters) to regulate fluid flow, reduce energy consumption, and lower costs. Various configurations—such as hydrodynamic flow focusing, staggered herringbone micromixers, bifurcating mixers, T-junction mixers, and baffle mixers—enhance control over the mixing environment by tailoring flow in narrow channels.[25] These configurations are particularly advantageous for precise formulations, even for expensive drugs, although the small channel sizes can limit scalability.

Flow dynamics and mixing conditions are critical in MNP. The physics of surface and interface interactions plays a pivotal role in MNP. At the nanoscale, the high surface-to-volume ratio amplifies interfacial forces, significantly impacting particle formation and stabilization. Surface tension (γ) governs the interfacial energy, while the interfacial curvature determines the Laplace pressure, influencing nanoparticle size and shape. The balance between cohesive forces (within the liquid) and adhesive forces (between liquid and solute) drives nucleation and growth processes.[73]

In the confined microchannels of MNP, the interplay of diffusion and interfacial tension creates a uniform solute distribution, enhancing the nucleation rate. Additionally, wetting properties, characterized by the contact angle (θ), influence solvent and anti-solvent interactions, affecting particle morphology. Hydrophilic channel walls promote spreading and mixing, while hydrophobic surfaces may induce localized aggregation due to poor wetting. The wettability of microfluidic channel walls significantly influences nanoprecipitation by affecting fluid mixing, solute diffusion, and particle formation. Hydrophilic surfaces ($\theta < 90°$) enhance solvent spreading, promote uniform solute distribution, and improve mixing efficiency, resulting in smaller and more homogeneous nanoparticles.[74] Conversely, hydrophobic surfaces ($\theta > 90°$) can lead to poor wetting, localized aggregation, and increased particle polydispersity due to inefficient mixing.[58] Furthermore, excessive hydrophobicity may cause nanoparticle adhesion to channel walls, leading to fouling and flow disturbances.[75] Optimizing wettability through surface modifications, such as plasma treatment or chemical coatings, can enhance process stability and ensure consistent nanoparticle synthesis.[76] Optimizing surface energy and flow conditions is crucial to ensuring uniform particle formation. Increasing the flow rate ratio between the solvent and anti-solvent promotes diffusion, generating more nucleation sites and resulting in smaller, more uniform PNPs.[61] Studies by Heshmatnezhad et al. and Chiesa et al. confirmed that higher total flow rates reduce particle size due to intensified shear forces, causing oversaturation and greater nucleation.[77–80] However, excessive flow rates can induce particle aggregation, leading to an increase in particle size at channel junctions, as demonstrated in the TEM images and DLS plot (Fig. 5(a)–(f)).[81] The Reynolds number (Re) also influences particle size; Liu et al. found that increasing Re enhanced turbulence, improving mixing until particle size stabilized. At lower drug-to-polymer ratios, thinner polymer shells formed around drug cores, while higher Re led
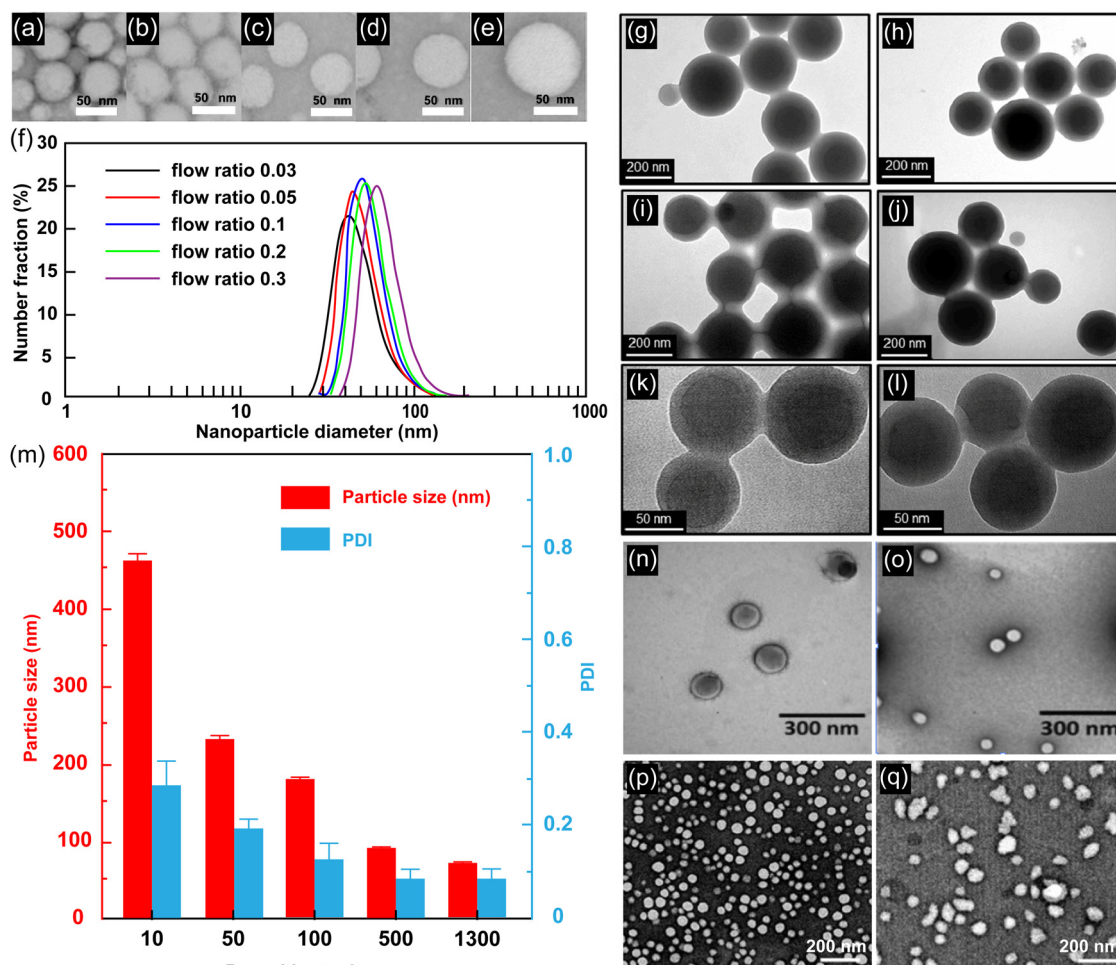
Fig. 5 (a)–(e) TEM images of PNPs prepared at flow rate ratios. The PNPs of mPEG-PLGA from the flow ratios of (a) 0.03, (b) 0.05, (c) 0.1, (d) 0.2, (e) 0.3. (f) Corresponding dynamic light scattering plots of PNPs.[81] (g)–(l) TEM images of the core–shell PNP synthesized by varying drug–polymer weight ratio and Reynolds number. (g) and (h) Drug–polymer weight ratio of 1 : 1 and Re of 100. (i) and (j) Drug–polymer weight ratio of 2 : 1 and Re of 100. (k) and (l) Drug–polymer weight ratio of 1 : 1 and Re 1300. (m) Particle size distribution and polydispersive index (PDI) as a function of Reynolds number.[82] (n) and (o) TEM images of PNPs prepared under varying flow rate ratios of (n) 1 : 1 and (o) 10 : 1.[59] (p) and (q) TEM images of PNPs as a function of drug (curcumin) to polymer ratio at (p) 0.5 and (q) 10.[5]

to smaller core–shell particles across different charged polymers (Fig. 5(g)–(m)).[82]

The material properties of microfluidic channels play a pivotal role in determining the outcomes of MNP by influencing fluid dynamics, mixing efficiency, and nanoparticle characteristics. Key material attributes such as wettability, surface charge, and mechanical properties directly impact the nucleation and growth processes of nanoparticles. The wettability of channel materials, defined by their surface energy, affects fluid flow patterns and mixing behavior within microchannels. Hydrophilic materials, characterized by high surface energy, promote effective solvent spreading and facilitate uniform solute distribution. This leads to enhanced mixing efficiency and results in the formation of smaller, more homogeneous nanoparticles. In contrast, hydrophobic materials with low surface energy can cause inadequate wetting, leading to poor mixing and localized solute concentration gradients. These conditions may result in the formation of larger, polydisperse

nanoparticles due to uneven nucleation rates. For instance, the use of PDMS in microfluidic devices has been shown to influence nanoparticle synthesis outcomes due to its inherent hydrophobicity.[83]

The surface charge of channel materials influences electrostatic interactions between the channel walls and the solute particles. Materials with surface charges that are compatible with the solute can prevent unwanted adsorption of nanoparticles onto the channel walls, thereby reducing fouling and ensuring a stable nanoprecipitation process. Conversely, incompatible surface charges can lead to particle adhesion, affecting the yield and quality of the nanoparticles produced. The chemical compatibility between the channel material and the solvents used is also crucial, as interactions at the interface can alter the physicochemical properties of the forming nanoparticles. Additionally, the mechanical strength and thermal conductivity of channel materials determine their ability to withstand operational conditions without deforming

or degrading. Materials with high mechanical strength maintain structural integrity under various flow rates and pressures, ensuring consistent nanoparticle synthesis. Thermal properties influence heat dissipation within the microchannels, affecting solvent evaporation rates and, consequently, the supersaturation levels critical for controlled nanoprecipitation. Materials like PDMS, commonly used in microfluidic devices, offer flexibility and ease of fabrication but may have limitations in mechanical and thermal stability under certain conditions.[58] To optimize MNP outcomes, surface modification techniques are employed to tailor the material properties of microfluidic channels. Methods such as plasma treatment, chemical grafting, or coating with hydrophilic polymers can enhance surface wettability, improving fluid mixing and nanoparticle uniformity. These modifications can also introduce desired surface charges or functional groups, reducing particle adhesion and fouling. For example, treating PDMS surfaces to increase hydrophilicity has been shown to improve nanoparticle synthesis by promoting better mixing and reducing aggregation.[83]

Precise control over flow dynamics and channel design allows for fine-tuning of the nanoprecipitation process. The ratio of flow rates between solvent and anti-solvent governs mixing efficiency and interfacial area generation, both critical for particle nucleation. For instance, high flow rates create thinner diffusion layers, reducing interfacial resistance and promoting rapid saturation of solute molecules. At the same time, the Re dictates whether flow remains laminar or transitions to turbulent, with laminar flow providing the most reproducible conditions for nanoprecipitation.[84] Channel geometry, including T-junctions, staggered herringbone micromixers, and bifurcating designs, determines shear rates and residence times. Shear rates at the interface influence interfacial stability, where excessive shear can disrupt particle formation or cause aggregation.[85,86] Scaling up these designs while maintaining optimal mixing conditions remains a challenge due to the complex interplay of surface forces and flow dynamics. Fig. 5(n) and (o) illustrates the effect of flow rates on NP size, showing that increasing the flow rate reduces NP size.[59] Silverman et al. demonstrated that increasing drug-to-polymer ratios in poly(caprolactone)-*block*-poly(ethylene glycol) NPs primarily affected polydispersity. At the same time, particle size changed only slightly due to curcumin's plasticizing effect, as shown in TEM images (Fig. 5(p) and (q)).[5] Ma et al. showed that surfactant ratios affect particle morphology in nanopesticides.[66] The chemical composition of surfactants and stabilizers significantly influences interfacial properties during MNP. Surfactants reduce interfacial tension, stabilizing newly formed nanoparticles by preventing coalescence or Ostwald ripening. For example, ionic surfactants provide charge stabilization, while non-ionic surfactants rely on steric hindrance to maintain particle dispersion. The choice of surfactant must balance these stabilization mechanisms to achieve desired particle properties, particularly under varying flow rates and solvent compositions. Additionally, interfacial rheology—describing the deformation and flow of the interface—determines the stability of emulsions formed during nanoprecipitation. For instance, interfacial elasticity resists deformations under shear,

preventing coalescence in high-shear environments such as those in microfluidic channels.

FNP and MNP both enable controlled production of PNPs but differ significantly in their methodologies and applications. FNP is characterized by rapid mixing in a confined space, producing particles with narrow size distributions and high loading efficiency, particularly suitable for hydrophobic drugs. However, FNP has limitations in processing water-soluble biomolecules and often requires high-pressure pumps, which increase operational complexity. In contrast, MNP leverages ultra-low volumes and precise control over flow rates within microchannels, allowing for highly reproducible particle sizes and morphologies through laminar flow and diffusion-driven mixing. MNP excels in its fine-tuning capabilities, accommodating various solvent compositions and complex surfactant systems, making it ideal for applications requiring small-scale, precise formulations. While MNP offers high precision and low energy consumption, it faces challenges in scalability due to the small channel size. FNP, by contrast, can more readily accommodate larger production scales, albeit with less precise control over certain particle properties. Both methods are versatile tools in nanoparticle synthesis, with FNP favored for rapid production and MNP for applications demanding intricate control over nanoparticle characteristics. From an interfacial physics perspective, FNP operates under conditions of high interfacial tension and rapid mixing, which can lead to kinetic control over particle size but may limit precision. In contrast, MNP emphasizes interfacial control through diffusion-driven mixing, allowing finer tuning of particle characteristics.[36] The lower interfacial tension achieved in MNP setups, often facilitated by surfactants or solvent composition, supports the formation of more uniform nanoparticles. For instance, in MNP, the relationship between surface energy and flow velocity can be optimized to achieve a balance between nucleation and growth, ensuring monodispersity. Meanwhile, FNP relies on intense mixing to overcome interfacial resistance, often resulting in broader size distributions.[87]

Other mixing techniques for controlling nanoprecipitation

Recently, new techniques have emerged to enhance the mixing between solvent and anti-solvent phases in nanoprecipitation processes.[88] One such method, electrohydrodynamic (ED) mixing, achieves turbulent mixing through an applied voltage that triggers the nanoprecipitation process.[89,90] Unlike flash nanoprecipitation (FNP), which relies on high flow rates of solvent and anti-solvent to induce turbulence and achieve homogeneous mixing, ED mixing uses an electric field to create similar mixing conditions at significantly lower flow rates. The applied voltage generates an electric field that promotes turbulent mixing, resulting in nanoparticle formation with precise control over particle size.

Microfluidic platforms, such as Y-junction mixers, have demonstrated precise control over mixing dynamics, leading

to uniform NPs synthesis with high reproducibility.[91] The application of staggered herringbone micromixers further enhances mass transfer efficiency, facilitating the synthesis of metal–organic frameworks (MOFs) with tunable porosity and controlled drug release.[92] Beyond microfluidic devices, high-speed homogenization remains an effective approach for achieving rapid solvent-exchange-driven nanoprecipitation, yielding lipid–polymer hybrid nanoparticles with enhanced colloidal stability and encapsulation efficiency.[58] Additionally, ultrasonic-assisted nanoprecipitation has been employed for the synthesis of bioactive metal–organic frameworks, enabling targeted and responsive drug delivery applications.[93] Electro-hydrodynamic mixing techniques, including jetting-based nanoprecipitation, have further optimized particle formation by leveraging charge-induced forces, leading to highly monodisperse NPs for biomedical applications. The potential of these techniques is evident in diverse fields, from drug delivery to energy storage, where precise NPs control is critical.[94] These advancements in nanoprecipitation mixing techniques highlight the growing role of controlled microenvironment engineering in NPs synthesis, offering new opportunities for enhanced functionality and efficiency.

Membrane nanoprecipitation is another method for producing polymer-based nanoparticles, where mixing occurs directly at the pores of a membrane.[95] In this method, an organic solvent and anti-solvent are introduced on opposite sides of a membrane with defined pore structures. Mixing occurs at these pores, enabling nanoparticle formation by regulating solvent diffusion. For example, the organic solvent may occupy the shell side of the membrane, mixing with the anti-solvent in the lumen side, or *vice versa*, driven by a pressure gradient. Membrane properties, particularly pore size and wettability, significantly influence particle size and polydispersity. Despite its precision, membrane nanoprecipitation faces challenges in scaling up due to the limited availability of suitable membranes with defined pore characteristics.

Electrospray nanoprecipitation combines solvent-shifting techniques with electrospray to synthesize polymer nanoparticles (PNPs).[96,97] In this process, the polymer solution is pumped through a nozzle connected to a high-voltage power supply, generating charged droplets that are subsequently mixed with a non-static aqueous phase under stirring. The electric field controls droplet size, facilitating rapid solvent evaporation, oversaturation, and nanoparticle formation. This technique produces monodisperse, surfactant-free nanoparticles, allowing for precise control over particle characteristics.

Techniques such as UV-vis absorption, Raman spectroscopy, and fluorescence can be employed in microfluidic channels to monitor the particle formation process in real-time. By coupling these spectroscopic methods with machine learning algorithms, we can dynamically adjust parameters like flow rates, solvent composition, and temperature to maintain consistent particle size and morphology. Additionally, dynamic light scattering (DLS) and *in situ* light scattering or particle tracking microscopy offer real-time monitoring of particle size distribution and growth dynamics. Temperature control and monitoring within the microfluidic system ensures consistent reaction kinetics, while solvent composition monitoring provides further precision in maintaining optimal conditions for nanoprecipitation. This integration enhances reproducibility and scalability, providing a precise and adaptable framework for controlling nanoprecipitation and producing nanoparticles with tailored properties.

For systems involving metal-based nanoparticle synthesis, electrochemical techniques such as cyclic voltammetry (CV) or electrochemical impedance spectroscopy (EIS) can be employed to monitor ion reduction and redox processes. These methods are particularly effective in controlling the nucleation and growth of metal nanoparticles, enabling real-time adjustments to ion concentrations, pH, and other critical parameters in metal nanoprecipitation processes.

Physicochemical properties of polymers and solvents in nanoprecipitation

The interaction between the organic phase, aqueous phase, and the solute molecules plays a crucial role in determining the size and properties of polymer nanoparticles (PNPs) in nanoprecipitation.[16] This can be understood by considering the diffusivity of the organic phase in the aqueous phase, which influences the distribution of solute molecules. A decrease in the diffusion rates of the organic and aqueous phases results in an increase in particle size. Moreover, as the affinity or interaction between the aqueous and organic phases increases, the resulting PNPs tend to have smaller sizes.[98–100]

Additionally, the interaction between the organic phase and the solute molecules determines the quality of the solvent for a given polymer, whether it is a good or poor solvent. In the case of a good solvent for a polymer, the resulting particle size tends to be larger due to the extended conformation of the solute molecules. Conversely, in a poor solvent, the solute molecules collapse, resulting in smaller particle sizes. Since these interactions vary for different solvents, the size and properties of the PNPs also change with variations in the organic phase.

This section will discuss the effects of polymer characteristics (such as concentration, molecular weight, and degree of hydrophobicity) and solvents on the size and properties of nanomaterials. The variation in particle properties with changes in solution parameters in nanoprecipitation techniques is summarized in Table 1.

The interactions between the organic phase, aqueous phase, and solute molecules are crucial in determining the size and characteristics of polymer nanoparticles (PNPs) in nanoprecipitation.[16] The diffusivity between phases influences the distribution of solute molecules: slower diffusion typically results in larger particles, while stronger affinity between the phases tends to reduce particle size. Furthermore, the interaction between the organic phase and solute molecules determines the solvent quality for a given polymer. In the case of good solvents, which extend the polymer chains, larger particles are typically

Table 1 Comparison of mixing techniques: batch, flash, and microfluidic

Mixing technique	Advantages	Disadvantages	Ref.
Batch	– Simple setup and easy to scale up – Suitable for large volumes – Cost-effective	– Longer mixing times – Poor control over mixing conditions – Higher batch-to-batch variability	101 and 102
Flash	– Rapid mixing – Suitable for high-throughput processes – Reduces aggregation in nanoparticle synthesis	– Requires precise control of flow rates – Limited to specific reaction conditions – Equipment may be expensive	67 and 103
Microfluidic	– Excellent control over mixing parameters – High reproducibility – Suitable for small volumes and lab-on-a-chip applications	– Low throughput – Complex fabrication and operation – Higher initial costs	58 and 104

Table 2 Summary of particle size variation under different conditions

Condition	ACN/water flow rate ratios	Particle size (nm)	DLS mean diameter (nm)	PDI
Fig. 5(a)	0.03	47 ± 2.5	49 ± 2.9	0.131
Fig. 5(b)	0.05	48 ± 2.0	52 ± 1.7	0.097
Fig. 5(c)	0.1	54 ± 1.9	56 ± 2.6	0.080
Fig. 5(d)	0.2	62 ± 2.5	59 ± 1.2	0.069
Fig. 5(e)	0.3	74 ± 2.2	71 ± 1.2	0.092

formed, whereas poor solvents cause the polymer chains to collapse, resulting in smaller particles (Tables 2 and 3).

Polymer properties, such as concentration, molecular weight, and architecture, also significantly affect PNP size and stability. For instance, Slater et al. observed that increasing polymer concentration led to a reduction in PNP size and polydispersity for vinyl polymers, while polysaccharide nanoparticles exhibited the opposite trend, with particle size increasing as polymer concentration increased.[62,112] Additionally, J. H. Lee and colleagues found that higher lignin concentrations resulted in larger PNPs with increased polydispersity and surface charge.[50] Polymer architecture also influences nanoparticle stability. For example, Slater et al. found that branched polymers produced more stable PNPs than linear polymers, which tended to precipitate after synthesis.[62] Furthermore, Pustulka et al. reported that higher polymer hydrophobicity, measured by the water–octanol partition coefficient, enhanced PNP stability. Specifically, coefficients above 7 led to more stable particles that were resistant to rapid aggregation.[67]

Solvent choice plays a critical role in controlling PNP properties, influencing size, stability, and morphology. Rao and Geckeler[113] examined various solvent-based methods, highlighting how solvent evaporation and nanoprecipitation impact particle size through solvent diffusion rates and polymer–solvent interactions. Dwivedi et al.[114] explored nanoprecipitation and emphasized that the choice of solvent and its miscibility with water dictate the final nanoparticle size, with polar solvents like acetone yielding smaller particles due to rapid diffusion into the aqueous phase. Huang and Zhang[105] systematically studied factors affecting PLGA nanoparticle size and found that solvent diffusion coefficient strongly dictates size distribution, with solvents like acetonitrile producing finer nanoparticles compared to acetone or THF.

Additionally, Aubry et al. demonstrated that lower polymer concentrations in PMMA, combined with a high aqueous phase volume, resulted in PNPs with narrow size distributions. However, higher polymer concentrations led to the formation of a mixture of micro- and nanoparticles, in line with the Smoluchowski kinetic model.[115] Similarly, Bovone et al. observed that solvent type influences PNP growth dynamics. Initial dynamic aggregates, formed through polymer exchange, stabilize once the solvent-specific water fraction is reached, ultimately determining the final particle size.[45] Solvent effects have also been explored in microfluidic nanoprecipitation (MNP) systems; Donno et al. found that increasing polymer molecular weight and flow rate ratio in MNP reduced PNP size and increased surface charge, with larger particles forming in the presence of surfactants at higher viscosities.[116]

Surfactants and other additives further modulate PNP size and morphology by controlling particle interactions during formation. Luque-Alcaraz et al. studied chitosan-based PNPs and found that surfactant presence, polymer concentration, and solvent-to-non-solvent ratios significantly influenced particle characteristics. For example, the presence of Tween 80 as a surfactant reduced particle size, while the absence of surfactant led to larger, more irregular PNPs due to coalescence.[117] Heshmatnezhad et al. showed that combining surfactants like PVA and Tween 80 improved particle uniformity and prevented aggregation, resulting in smoother, smaller, and more stable PNPs. In contrast, PNPs formed without surfactants were larger, with rougher morphology and non-uniform distributions.[77]

Latest developments in green solvents and their impact on nanoprecipitation processes

Nanoprecipitation, a widely adopted technique for nanomaterial synthesis, depends on the rapid mixing of solvents and non-solvents to trigger supersaturation and nanoparticle formation. Traditionally, organic solvents like acetone, THF, and DMSO have dominated due to their miscibility with water and ability to dissolve diverse precursors. However, their toxicity, volatility, and environmental footprint have driven a shift toward greener alternatives, reshaping nanoprecipitation in recent years. The integration of green solvents into nanoprecipitation processes has garnered significant attention due to their potential to enhance sustainability and reduce environmental impact in

Table 3 BNP: effects of nanoprecipitation conditions on the size and morphology of the PNPs

Polymer	Organic/aqueous phase	Parameter varied	Size	Morphology
PEG-*b*-PLA, PEG-*b*-PLGA, or PEG-*b*-PCL	DMF, acetone, acetonitrile, THF, or DMSO/water	Organic solvents	50–100 nm	Spherical[45]
Poly(vinyl alcohol)	Methanol, ethanol, propanol, *tert*-butanol/water	Polymer concentrations, interaction parameters	50–300 nm	Spherical[16]
p(HPMA50-EGDMA)	Acetone/water	Polymer structure (linear and branched), temperature, volume of organic phase, NaCl	50–800 nm	Spherical[62]
Poly(lactic-*co*-glycolic acid)	Acetonitrile, acetone and tetra-hydrofuran (THF)/PVA aqueous solution	Polymer concentration, organic solvent, ionic strength of aqueous phase and temperature	80–3500 nm	Spherical[105]
Polystyrene	Acetone, chloroform, tetrahydrofuran and acetonitrile/Tween-40, Pluronic F-68	Polymer, surfactant, non-solvent	100 nm–3 μm	Spherical[106]
Cellulose acetates	Acetone/water	Concentrations of cellulose acetate	160–400 nm	Spherical and bean-shaped particles[107]

FNP: effects of nanoprecipitation conditions on the size and morphology of the PNPs.

Polymer	Organic/aqueous phase	Parameter varied	Size	Morphology
Polystyrene	Tetrahydro-furan/water	Time, molecular weight, solution concentrations, stirring rate, solvent/non-solvent ratio	60–200 nm	Spherical[15]
Poly(ethylene glycol)-*block*-poly(ε-caprolactone)	Tetrahydro-furan and dimethyl sulfoxide (DMSO)/water	Solvent/non-solvent ratio, stream velocity	20–80 nm	Spherical[65]
Poly(3-hydroxybutyrate-*co*-3-hydroxyvalerate)	Dichloro-methane/SDS and PVA solutions	Polymer and surfactant concentrations	100–600 mm	Spherical[53]
PEG-*b*-PLGA, PS(10k)-*b*-PEG, PEG-*b*-PLA	Tetrahydro-furan/water	Nanoparticle concentrations	60–180 nm	Spherical[67]
PEO-*b*-PS, PEG-*b*-PCL	Tetrahydro-furan/water	Reynolds number	25–500 nm	Spherical[108]
PS-*b*-PI	Tetrahydro-furan/water	Polymer concentrations, chain length	30–300 nm	Spherical particles with concentric shells or a disordered lamellar[109]

MNP: effects of nanoprecipitation conditions on the size and morphology of the PNPs.

Polymer	Organic/aqueous phase	Parameter varied	Size	Morphology
Poly(methyl methacrylate) (PMMA)	Tetrahydrofuran/water	Polymer concentrations, volume flow rate ratio between water and the polymer solution	100–200 nm	Spherical[72]
Poly(lactic-*co*-glycolic acid)	Dimethylformamide/water	Micro-channel geometry, aspect ratio	50–300 nm	Spherical[59]
Pluronic F127	Tetrahydrofuran/water	Drug to polymer concentrations, flow rate, mixing time	70–200 nm	Spherical[110]
PLGA	Dimethylformamide (DMF) and tetrafluoroethylene/water	Flow rate	50–250 nm	Spherical[60]
PLGA-lipid-NPs	Tetrafluoroethylene (TFE) and 0.7 mL dimethylformamide (DMF)/water	Flow rate	60–90 nm	Spherical[111]
Polycaprolactone	THF and DMF/PVA solution	Flow rate ratio and total flow rate	100–300 nm	Spherical[77]

nanomaterial synthesis. These eco-friendly solvents not only minimize the use of hazardous chemicals but also offer unique physicochemical properties that can influence the characteristics of the resulting nanoparticles.

Deep eutectic solvents (DESs) have emerged as promising alternatives to traditional organic solvents in nanoprecipitation. Comprising a mixture of hydrogen bond donors and acceptors, DESs exhibit low volatility, biodegradability, and tunable solubility parameters. Their unique properties facilitate the efficient extraction of bioactive compounds from natural sources, which can subsequently act as reducing and stabilizing agents in nanoparticle synthesis. For instance, Vorobyova *et al.* demonstrated the use of a DES-based plant extract for the biosynthesis of silver nanoparticles, highlighting the solvent's role in enhancing nanoparticle stability and antibacterial efficacy.[118] Similarly, ionic liquids (ILs) particularly those based on imidazolium cations, have been extensively studied for their role in stabilizing nanomaterials during synthesis. Their negligible vapor pressure, thermal stability, and ability to dissolve a wide range of compounds make them suitable candidates for green nanoprecipitation processes. ILs can act as both solvents and stabilizing agents, influencing nanoparticle size, morphology, and dispersion stability. Tshemese *et al.* reviewed the application of imidazolium-based ILs in nanomaterial stabilization, emphasizing their potential to replace conventional, more hazardous solvents.[119]

The utilization of solvents derived from renewable biological sources, such as plant extracts and natural surfactants, aligns with the principles of green chemistry. These solvents often contain bioactive compounds capable of reducing metal ions and stabilizing nanoparticles. For example, sophorolipids, which are glycolipid biosurfactants, have been employed in flash nanoprecipitation techniques to construct nanodelivery systems. Their natural origin and biodegradability make them attractive alternatives to synthetic surfactants in nanoparticle formulation.[66] The incorporation of green solvents into nanoprecipitation processes offers several advantages such as (i) environmental sustainability: green solvents reduce the reliance on toxic organic solvents, thereby decreasing environmental pollution and health hazards,[120] (ii) enhanced biocompatibility: nanoparticles synthesized using bio-based solvents often exhibit improved compatibility for biomedical applications due to the absence of harmful residues,[121] and (iii) controlled nanoparticle characteristics: the unique properties of green solvents, such as viscosity and polarity, can be tailored to control nanoparticle size, morphology, and dispersion, which are critical parameters in various applications.[122] The adoption of green solvents in nanoprecipitation processes represents a significant advancement in the sustainable synthesis of nanomaterials. Ongoing research in this area is expected to further optimize these processes, leading to environmentally friendly and efficient production of nanoparticles for diverse applications.

Advanced nanostructures synthesized *via* nanoprecipitation

Nanoprecipitation is a highly advantageous technique for synthesizing drug delivery nanocarriers, making it a preferred method in pharmaceutical applications. Its simplicity, scalability, and ability to produce nanoparticles with controlled size and high drug loading make it suitable for encapsulating a wide range of active pharmaceutical ingredients, from small hydrophobic drugs to complex biomolecules. Additionally, nanoprecipitation is a solvent-efficient process with minimal energy requirements, which lowers production costs and reduces environmental impact. However, the technique does have limitations: it is primarily effective for hydrophobic drugs, as hydrophilic molecules tend to diffuse rapidly into the aqueous phase, leading to poor encapsulation efficiency and rapid drug leakage.[123] To address this challenge, various strategies have been explored. One common approach is to modify the polymer matrix by introducing amphiphilic copolymers, such as PEG, which enhances the solubility and interaction of hydrophilic drugs with the nanoparticle core.[124] Another strategy involves forming polyelectrolyte complexes, where oppositely charged polymers interact with hydrophilic drugs to stabilize encapsulation.[125] Additionally, the use of hydrophobic ion pairing has been employed, wherein hydrophilic drugs are complexed with counterions to temporarily enhance their hydrophobicity, improving retention within the nanoparticle matrix.[126] For example, hydrophobic ion pairing of heparin with surfactant-like cations has

been shown to significantly improve its encapsulation efficiency in polymeric nanoparticles.[127] Despite these advancements, optimizing formulation parameters, such as solvent selection, polymer–drug compatibility, and mixing conditions, remains crucial for achieving stable and efficient encapsulation of hydrophilic molecules.

Nanoprecipitation is particularly advantageous for hydrophobic drugs, improving their solubility and bioavailability. Yang *et al.* utilized salt-induced precipitation to achieve high drug loading (66.5% w/w) for hydrophobic drugs. By varying salt concentrations, they controlled particle size and aggregation, resulting in uniformly dispersed nanoparticles (50 nm) with high loading efficiency in high-salt conditions (Fig. 6(d)–(g)).[128] Liu *et al.* created stable core–shell PNPs with loading up to 58.5% by adjusting polymer precipitation timing, allowing for either single-core or multi-core formations depending on the desired release profile.[129] For the antioxidant drug astaxanthin, Azaman *et al.* encapsulated it in PLGA nanoparticles, producing stable and homogeneous PNPs (142 nm), optimized for enhanced oral bioavailability and antioxidant efficacy.[130]

Batch nanoprecipitation (BNP) has proven effective for encapsulating proteins and peptides, which benefit from controlled release. Chopra *et al.* developed insulin-loaded PLGA–PEG PNPs using BNP, achieving a tenfold increase in insulin loading while maintaining small particle size. The encapsulated insulin retained its structure, promoting long-term stability (Fig. 6(a)–(c)).[131] Zada *et al.* used BNP in a non-aqueous setup for nasal insulin delivery, yielding rapid release rates with nearly 50% of the drug released within the first hour, ideal for nasal administration where quick absorption is advantageous.[132]

Flash nanoprecipitation (FNP) has shown success in stabilizing hydrophobic drugs with complex release profiles. A "complex release profile" refers to a non-uniform or multi-phase drug release behavior over time, characterized by an initial burst followed by sustained, delayed, controlled, extended, or environment-responsive release. This behavior is influenced by factors such as drug–polymer interactions, nanoparticle composition, and external environmental conditions (*e.g.*, pH, temperature), making it critical for optimizing therapeutic efficacy. In this context, FNP enables precise control over nanoparticle formation, facilitating tailored drug release kinetics. Li *et al.* numerically studied the effect of solution/water flow rate ratios and microfluidic device geometry on mixing time. Fig. 6(h)[133] shows the microfluidic nanoprecipitation of curcumin nanoparticles. In the first stage, most of the polymer precipitates, forming polymeric NPs, followed by curcumin NPs. Some are stabilized by mPEG-PLGA, creating drug-loaded NPs. However, at higher curcumin concentrations, theres insufficient mPEG-PLGA to stabilize the drug NPs, leading to aggregation and microchannel blockage. To improve drug loading and stability, its ideal to precipitate the drug first, ensuring enough polymer is available to stabilize the NPs. Thus, the precipitation times for the polymer and drug should be aligned.[133] Qi *et al.* used FNP to encapsulate celastrol, achieving tunable drug loading (11–63%) in dextran-based PNPs. The formulation exhibited controlled release and reduced cytotoxicity toward liver cells,
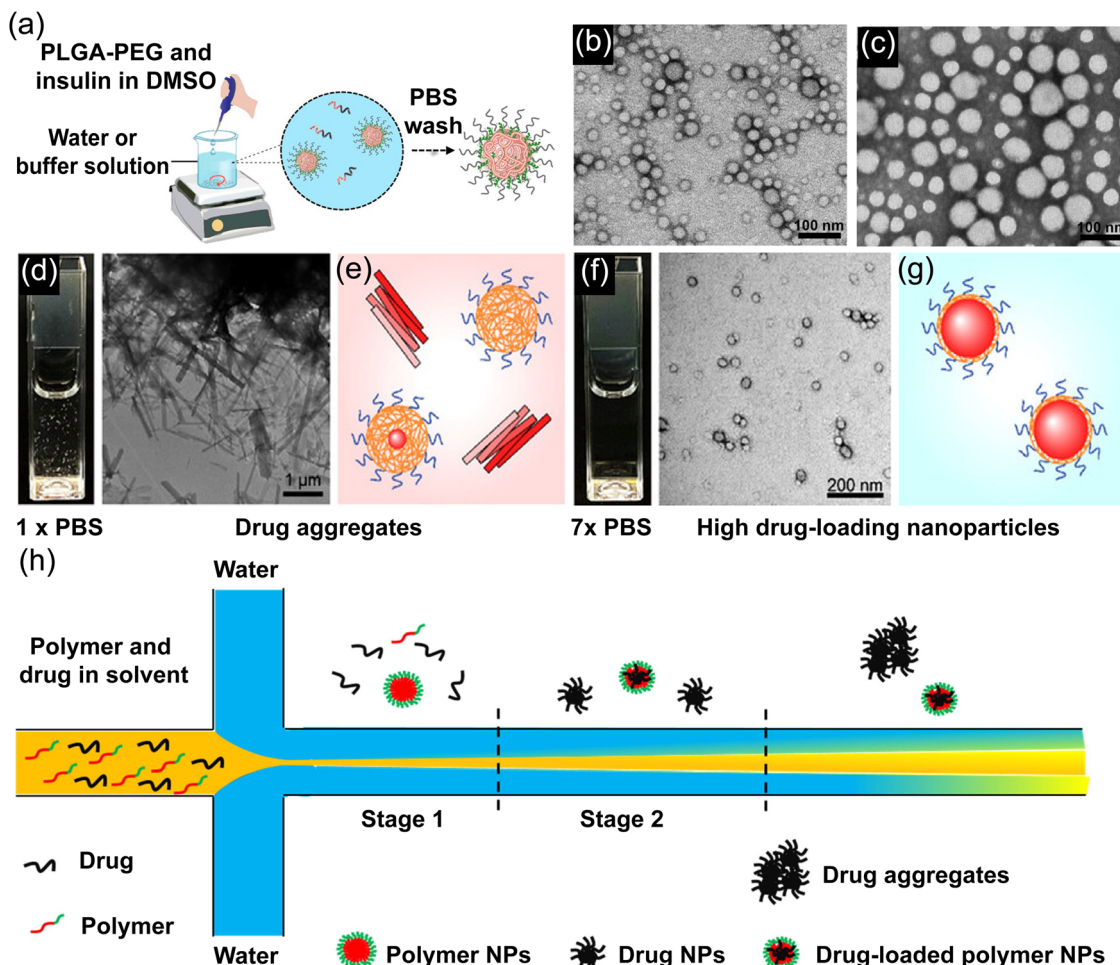
Fig. 6 Nanoprecipitation for fabrication of nanocarriers of pharmaceutical active ingredients. (a) Schematic representation of the preparation of the insulin-loaded PNPs (Ins-NPs). (b) TEM images of Ins-NPs and (c) PLGA−PEG NPs without insulin.[131] (d) The snapshot of the mixtures, TEM images, and schematic for the nanoparticles produced by (d) and (e) bad salt concentration and (f) and (g) good salt concentration in producing 50 wt% docetaxel-loaded PLGA10k−PEG5k nanoparticles.[128] (h) Schematic representation of the formation of the polymer-stabilized peroxide antimalarial drug nanoparticle and the drug release profile of the nanoparticle and unencapsulated powder in the bio media.[81]

with effective inhibition of lung cancer cells, demonstrating potential for targeted cancer therapies.[134]

Caggiano et al. employed FNP with confined impinging jets to co-encapsulate cannabidiol (CBD) and iron oxide. This design increased particle density, improving sedimentation for controlled release studies. Stabilized with HPMCAS or lecithin, the nanoparticles demonstrated enhanced dissolution, with HPMCAS-coated particles releasing six times faster in intestinal media compared to bulk CBD as shown in Fig. 7(a).[135] Zeng et al. utilized a scalable approach to prepare lipid-coated solid drug (methotrexate) nanoparticles by combining flash nanoprecipitation and extrusion techniques (Fig. 7(b)), optimizing individual steps and providing flexibility in selecting nanoparticle surface functionalities.[136] Ye et al. encapsulated the cancer drug paclitaxel within PEG-PLA/zein nanoparticles using FNP, achieving high encapsulation efficiency (up to 78.1%) and controlled, sustained release. The presence of zein promoted hydrophobic interactions, allowing slow release at acidic pH, advantageous for tumor-targeted delivery.[137]

Microfluidic nanoprecipitation (MNP) enables precise control over particle size, ideal for creating pH-responsive nanocarriers. Li et al. synthesized PEG-PLGA PNPs for curcumin delivery, achieving a loading capacity of 2.6% and 77.3% encapsulation efficiency. However, they observed particle aggregation at higher curcumin concentrations, highlighting the importance of concentration control for stable dispersions.[81] Baby et al. developed pH-responsive shellac nanoparticles for curcumin delivery using MNP, achieving up to 50% drug loading. At neutral pH, the nanoparticles released 28% of the drug in 4 hours, increasing to 51% over 51 hours, demonstrating suitability for sustained release in response to pH changes.[80] The pH-responsive capabilities of FNP were further explored by Qi et al., who used dextran-based PNPs to encapsulate celastrol, an anti-cancer drug. The PNPs achieved adjustable drug loading (11–63%) with effective release, reduced liver toxicity, and significant inhibition of lung cancer cells. This adaptable release profile shows promise for personalized cancer therapies.[134]
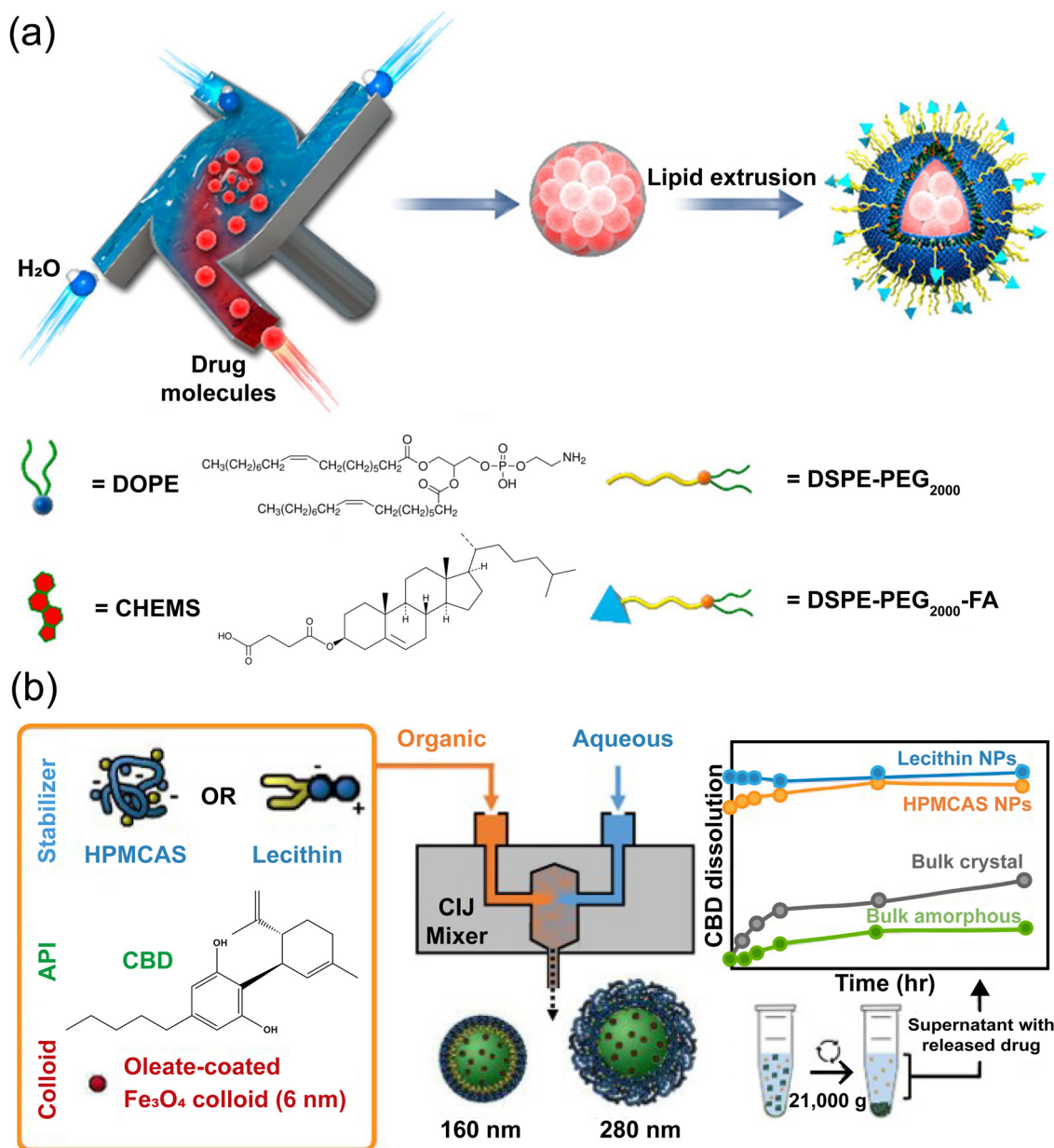
Fig. 7 (a) Schematic representation of the preparation of drug-loaded nanoparticles and the comparative *in vitro* release profile of drug-loaded nanoparticles with bulk crystalline and bulk amorphous CBD in fed-state simulated intestinal media,[136] (b) cartoon representing the microfluidic nanoprecipitation method to synthesize the curcumin-loaded block co-polymer.[135]

Future research could focus on enhancing nanoprecipitations versatility for hydrophilic drugs by developing novel polymer–drug conjugates or exploring stimuli-responsive polymers that adapt to various biological environments. Other promising avenues include optimizing process parameters to improve the encapsulation efficiency and stability of delicate biomolecules, such as proteins and peptides, and scaling up microfluidic-based nanoprecipitation methods. Furthermore, exploring the use of eco-friendly solvents and biodegradable polymers can make nanoprecipitation more sustainable, aligning with green chemistry goals. Addressing these areas could further enhance the applicability and impact of nanoprecipitation in drug delivery.

Other advanced structures: nanocrystals, semiconductor nanoparticles, vesicles, core–shell, and porous nanoparticles

Nanoprecipitation is a versatile technique widely employed for synthesizing not only polymer nanoparticles (PNPs) but also a variety of advanced nanostructures, such as nanocrystals, semiconductor nanoparticles, vesicles, core–shell particles, porous nanoparticles, and semiconducting polymer nanoparticles. These nanostructures, depicted in Fig. 8, have applications in
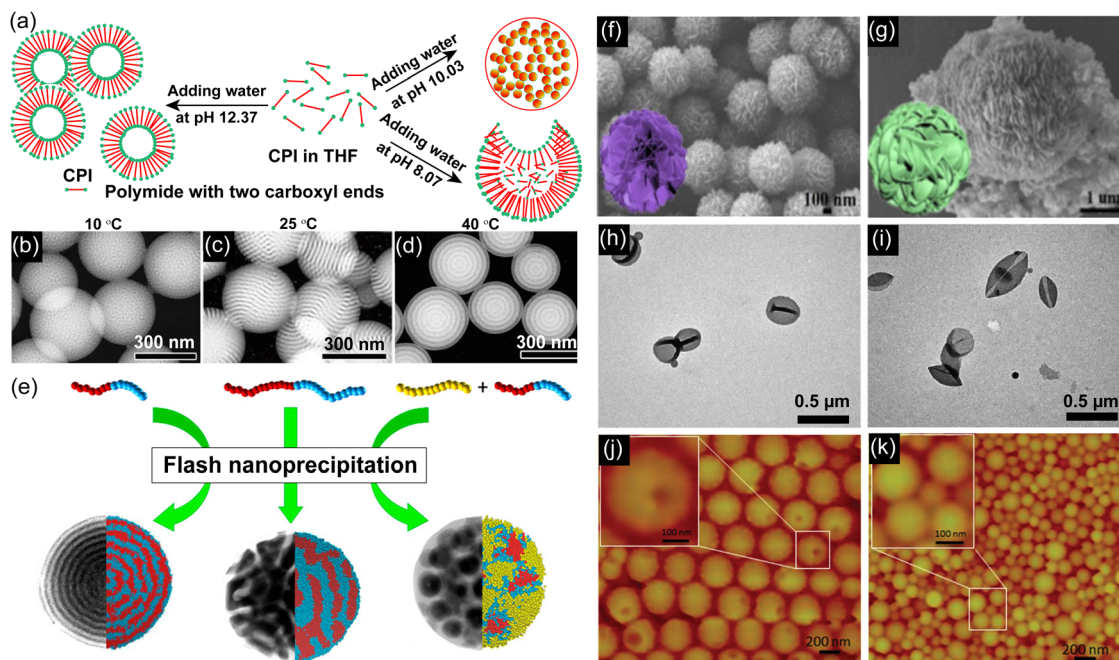
Fig. 8 (a) Complex morphologies through mono-component PNPs obtained by varying the solution pH.[140] (b)–(d) Effect of temperature on morphology of the PNPs.[141] (e) Schematic illustration of the Janus colloid formed from a blend of homo and block co-polymers solutions.[109] (f) and (g) SEM images of the particles of different morphologies (f) MoDo-SiO$_2$ and (g) CTS-MoDo-SiO$_2$.[142] (h) and (i) TEM images of organosilica nanoparticles (h) collapsed hollow structure with intrinsic flexibility and deformation. (i) Ultra-thin shells with deformable hollow structure[14] (j) and (k) AFM images of the polymer Janus nanoparticles obtained using (j) thiol-PLGA (k) PLA/PGA solutions.[143]

fields ranging from opto-electronics and biosensing to bioimaging, catalysis, and drug delivery.[9,10,12,14,138,139] Nanoprecipitation simplifies the synthesis of nanomaterials that benefit from controlled solvent-based assembly, particularly where low energy input and single-step synthesis are required. This makes it an ideal method for producing nanostructures that would otherwise be difficult or inefficient to achieve using traditional techniques.

Nanocrystals are crystalline nanoparticles with a wide range of potential applications in opto-electronics, biosensing, bioimaging, and catalysis due to their enhanced dissolution rates and tunable physicochemical properties.[13,144,145] Their properties can be customized by selecting appropriate stabilizing agents, and nanoprecipitation offers a simple yet effective synthesis method.[146,147] For example, Xu et al.[147] used nanoprecipitation to create aggregation-induced emission (AIE) activated nanocrystals for super-resolution imaging. These AIE nanocrystals exhibited enhanced brightness and photostability, making them ideal for stimulated emission depletion nanoscopy. This technique improved the resolution of lysosomal imaging and enabled dynamic tracking of lysosomal motion over extended periods, surpassing standard confocal microscopy capabilities. Thakkur et al.[148] employed electrospray nanoprecipitation to produce docetaxel nanocrystals, which showed a significant increase in dissolution rates (77% vs. 30% for bulk docetaxel) due to their high surface area. In vivo studies demonstrated effective tumor load reduction in a lung cancer model, underscoring the therapeutic potential of nanocrystals in oncology.

Semiconducting polymer nanoparticles (SNPs) are emerging materials with applications in sensing, imaging, and diagnostics, owing to their fluorescence, biocompatibility, and superior optical and photothermal properties compared to traditional dyes.[12,139,149] The molecular structure of the semiconducting polymers largely determines the properties of the SNPs. Holmes et al.[12] synthesized Janus SNPs with electron- and hole-accepting faces using batch nanoprecipitation. These Janus SNPs were employed to fabricate organic field-effect transistors, demonstrating efficient charge transport across thin films, highlighting their potential in optoelectronic applications. He et al.[54] used flash nanoprecipitation (FNP) to synthesize ultra-small polymer dots (less than 10 nm) with narrow size distribution and tunable optical properties. By selecting polymers such as MEH-PPV, PFBT, and PFPV, they achieved highly bright and stable polymer dots suitable for high-resolution imaging. The size of these polymer dots was controlled by adjusting the polymer type and precursor concentration, showcasing the flexibility of FNP for tailoring nanoparticle properties.

Pu et al.[150] developed low-bandgap diketopyrrolopyrrole (DPP) SNPs for in vivo photoimaging. DPP, known for its photostability and thermal stability, was copolymerized with electron-donating monomers to fine-tune band gaps, resulting in stable SNPs (45 nm) with modifiable fluorescence and photoacoustic properties. By adjusting the donor–acceptor composition, they optimized SNPs for photothermal applications, enhancing photothermal conversion efficiency while reducing fluorescence. This tunable property makes DPP SNPs particularly promising for biomedical imaging and therapy.

Wang et al.[140] demonstrated that vesicles, porous spheres, and dimpled beads could be synthesized by controlling the pH of an aqueous solution of carboxyl-terminated polyimide (Fig. 8(a)). At pH 8.07, the polymers aggregated into dimpled beads (100–600 nm), while increasing the pH to 10 produced smooth, spherical particles (100–200 nm). This pH-dependent assembly highlights how solution conditions can direct nanoparticle morphology (Fig. 8(b)–(d)). Similarly, Higuchi et al. used thermal annealing to induce disorder–order and order–order phase transitions in block copolymer nanoparticles (Fig. 8(b)–(d)). The unusual thermal behaviors suggest that the nanoparticle effect lowers the glass transition temperature of the block copolymer, likely due to the increased surface-area-to-volume ratio.[141]

Grundy et al.[109] synthesized colloids with complex internal structures by blending poly(styrene) and poly(styrene-b-isoprene) block copolymers in an FNP process. Low-molecular-weight copolymers produced concentric, onion-like shells, while higher molecular weights resulted in disordered, lamellar structures, demonstrating control over internal nanoparticle architecture through polymer selection (Fig. 8(e)). Shahnavas et al.[151] developed pH-sensitive core–shell nanoparticles composed of PLGA and carboxymethyl chitosan, allowing dual drug loading. Doxorubicin was loaded in the shell, while docetaxel was encapsulated in the core, creating a system responsive to environmental pH. The core–shell structure enabled controlled drug release: doxorubicin was released rapidly from the shell, while docetaxel in the core showed slower release, allowing for layered, sequential delivery.

Ma et al.[14] used a modified FNP setup to develop deformable hollow mesoporous organosilica nanoparticles (HMONs) with high surface area and tunable mechanical properties (Fig. 8(f)–(i)). By introducing disulfide bonds into the silica network, they created nanoparticles with lower Young's modulus, enabling deformation. Loaded with the model nanopesticide abamectin, these HMONs demonstrated improved insecticidal efficacy, showing their potential for applications in agriculture where controlled-release carriers are needed. In another work, Xie et al.[143] designed a fluidic nanoprecipitation system capable of fabricating biocompatible Janus polymeric nanoparticles made from the FDA-approved polymer poly(lactic-co-glycolic acid) (PLGA), as shown in AFM images (Fig. 8(j) and (k)). The system features dual inlets, each for one-half of the particle, which is inserted into the precipitation stream.

The possible future scope of nanoprecipitation includes AI and ML integration for predictive control over nanoparticle synthesis, automated and scalable processes using continuous-flow and microfluidic systems, and hybrid/multi-functional nanoparticles for advanced applications in drug delivery, sensing, and catalysis. These advancements will enhance precision, reproducibility, and scalability, making nanoprecipitation more efficient and versatile.

Conclusions

Nanoprecipitation is a simple, versatile, low-energy, and cost-effective method for synthesizing a wide variety of nanomaterials.

Its adaptability, coupled with precise control over physicochemical properties and mixing hydrodynamics, enables customized size, morphology, and internal structures of particles. This solution-based approach has evolved significantly, enabling the production of nanomaterials with distinct morphological characteristics. Through these capabilities, nanoprecipitation holds great promise for developing high-performance, multifunctional nanomaterials. As highlighted in this review, nanoprecipitations effectiveness across batch, flash, and microfluidic mixing configurations provides fine control over drug loading capacity, encapsulation efficiency, and release kinetics, making it a powerful approach for tailoring drug delivery systems.

Despite its potential, challenges persist, particularly in large volume of solvents, scaling microfluidic techniques and optimizing formulations for hydrophilic compounds. Future advancements in nanoprecipitation could address these limitations through several innovative approaches. First, the development of fast and efficient methods for concentrating and separating nanoparticles from large liquid volumes would streamline production, making the process more time-efficient. Second, extending nanoprecipitation techniques to include hydrophilic compounds could broaden its applicability across biomedical and industrial fields. Finally, the automation of nanoprecipitation through robotic systems, coupled with machine learning for optimizing formulation and flow conditions, could accelerate the discovery and development of new nanomaterial formulations.

List of abbreviations

BNP	Batch nanoprecipitation
CBD	Cannabidiol
DMF	Dimethylformamide
DMSO	Dimethyl sulfoxide
FNP	Flash nanoprecipitation
HMONs	Hollow mesoporous organosilica nanoparticles
HPMCAS	Hydroxypropyl methylcellulose acetate succinate
MNP	Microfluidic nanoprecipitation
PBS	Phosphate buffer solution
PDI	Polydispersive index
PEG-b-PLA	Poly(ethylene glycol)-block-poly(DL-lactide)
PNP	Polymer nanoparticle
PMMA	Poly(methyl methacrylate)
PLGA	Poly(lactic-co-glycolic acid)
PLGA	Poly(lactide-co-glycolide)
PVA	Poly(vinyl alcohol)
Re	Reynolds number
THF	Tetrahydrofuran
$PbSO_4$	Lead(II) sulfate

Data availability

No primary research results, software or code have been included and no new data were generated or analysed as part of this review.

Conflicts of interest

There are no conflicts to declare.

Acknowledgements

References

1 H. Fessi, F. Puisieux, J. P. Devissaguet, N. Ammoury and S. Benita, Nanocapsule formation by interfacial polymer deposition following solvent displacement, *Int. J. Pharm.*, 1989, **55**, R1–R4.

2 D. Quintanar-Guerrero, E. Allémann, H. Fessi and E. Doelker, Preparation techniques and mechanisms of formation of biodegradable nanoparticles from preformed polymers, *Drug Dev. Ind. Pharm.*, 1998, **24**, 1113–1128.

3 W. N. Sharratt, V. E. Lee, R. D. Priestley and J. T. Cabral, Precision polymer particles by flash nanoprecipitation and microfluidic droplet extraction, *ACS Appl. Polym. Mater.*, 2021, **3**, 4746–4768.

4 S. Hasankhan, M. Tabibiazar, S. M. Hosseini, A. Ehsani and M. Ghorbani, Fabrication of curcumin-zein-ethyl cellulose composite nanoparticles using antisolvent co-precipitation method, *Int. J. Biol. Macromol.*, 2020, **163**, 1538–1545.

5 L. Silverman, G. Bhatti, J. E. Wulff and M. G. Moffitt, Improvements in drug-delivery properties by co-encapsulating curcumin in SN-38-loaded anticancer polymeric nanoparticles, *Mol. Pharmaceutics*, 2022, **19**, 1866–1881.

6 S. I. Hamdallah, R. Zoqlam, B. Yang, A. Campbell, R. Booth, J. Booth, P. Belton and S. Qi, Using a systematic and quantitative approach to generate new insights into drug loading of PLGA nanoparticles using nanoprecipitation, *Nanoscale Adv.*, 2024, **6**, 3188–3198.

7 S. M. Ghasemi and S. S. Alavifar, The role of physicochemical properties in the nanoprecipitation of cellulose acetate, *Carbohydr. Polym.*, 2020, **230**, 115628.

8 R. Ahmed Bhutto, Z. Fu, M. Wang, J. Yu, F. Zhao, S. Khanal, A. Halepoto, J. Wang, M. A. Cohen Stuart and X. Guo, Facile controlling internal structure of β-carotene-loaded protein nanoparticles by flash nanoprecipitation, *Mater. Lett.*, 2021, **304**, 130523.

9 J. Li and K. Pu, Semiconducting polymer nanomaterials as near-infrared photoactivatable protherapeutics for cancer, *Acc. Chem. Res.*, 2020, **53**, 752–762.

10 A. Langlois, G. T. Mason, M. H. Nguyen, M. Rezapour, P.-L. Karsenti, D. Marquardt and S. Rondeau-Gagné, Photophysical and optical properties of semiconducting polymer nanoparticles prepared from hyaluronic acid and polysorbate 80, *ACS Omega*, 2019, **4**, 22591–22600.

11 R. Shu, Z. Han, A. Elsukova, Y. Zhu, P. Qin, F. Jiang, J. Lu, P. O. Persson, J. Palisaitis and A. Le Febvrier, *et al.*, Solid-state Janus nanoprecipitation enables amorphous-like heat conduction in crystalline Mg3Sb2-based thermoelectric materials, *Adv. Sci.*, 2022, **9**, 2202594.

12 A. Holmes, H. Laval, M. Schmutz, S. Blanc, J. Allouche, B. Watts, G. Wantz, N. Holmes, K. Hirakawa, E. Deniau, S. Chambon, C. Lartigau-Dagron and A. Bousquet, Janus organic semiconductor nanoparticles prepared by simple nanoprecipitation, *Mater. Today Chem.*, 2022, **26**, 101229.

13 Y. Sun, H. Gao, H. Zhang, F. Xu, W. You, G. Pan, H. Zhang, Z. Zhang and Y. Mao, Controllable synthesis of Sn0.33WO3 tungsten bronze nanocrystals and its application for upconversion luminescence enhancement, *Ceram. Int.*, 2023, **49**, 1128–1136.

14 E. Ma, Z. Fu, L. Sun, K. Chen, Z. Liu, Z. Wei, L. Li and X. Guo, Organosilica-based deformable nanopesticides with enhanced insecticidal activity prepared by flash nano-precipitation, *React. Chem. Eng.*, 2023, **8**, 1457–1463.

15 C. Zhao, S. Melis, E. P. Hughes, T. Li, X. Zhang, P. D. Olmsted and E. Van Keuren, Particle formation mechanisms in the nanoprecipitation of polystyrene, *Langmuir*, 2020, **36**, 13210–13217.

16 M. Beck-Broichsitter, Solvent impact on polymer nanoparticles prepared nanoprecipitation, *Colloids Surf., A*, 2021, **625**, 126928.

17 B. Misra, K. A. Hughes, W. H. Pentz, P. Samart, W. J. Geldenhuys and S. Bobbala, Flash nanoprecipitation assisted self-assembly of ionizable lipid nanoparticles for nucleic acid delivery, *Nanoscale*, 2024, **16**, 6939–6948.

18 X. Zhang, Z. Lu, H. Tan, L. Bao, Y. He, C. Sun and D. Lohse, Formation of surface nanodroplets under controlled flow conditions, *Proc. Natl. Acad. Sci. U. S. A.*, 2015, **112**, 9253–9257.

19 X. H. Zhang and W. Ducker, Formation of interfacial nanodroplets through changes in solvent quality, *Langmuir*, 2007, **23**, 12478–12480.

20 X. H. Zhang and W. Ducker, Interfacial oil droplets, *Langmuir*, 2008, **24**, 110–115.

21 Z. Lu, M. H. K. Schaarsberg, X. Zhu, L. Y. Yeo, D. Lohse and X. Zhang, Universal nanodroplet branches from confining the ouzo effect, *Proc. Natl. Acad. Sci. U. S. A.*, 2017, **114**, 10332–10337.

22 H. Tan, C. Diddens, P. Lv, J. G. Kuerten, X. Zhang and D. Lohse, Evaporation-triggered microdroplet nucleation and the four life phases of an evaporating ouzo drop, *Proc. Natl. Acad. Sci. U. S. A.*, 2016, **113**, 8642–8647.

23 H. Tan, C. Diddens, M. Versluis, H.-J. Butt, D. Lohse and X. Zhang, Self-wrapping of an ouzo drop induced by evaporation on a superamphiphobic surface, *Soft Matter*, 2017, **13**, 2749–2759.

24 Y. Liu, G. Yang, D. Zou, Y. Hui, K. Nigam, A. P. J. Middelberg and C.-X. Zhao, Formulation of nanoparticles using mixing-induced nanoprecipitation for drug delivery, *Ind. Eng. Chem. Res.*, 2020, **59**, 4134–4149.

25 S. J. Shepherd, D. Issadore and M. J. Mitchell, Microfluidic formulation of nanoparticles for biomedical applications, *Biomaterials*, 2021, **274**, 120826.

26 X. Yan, J. Bernard and F. Ganachaud, Nanoprecipitation as a simple and straightforward process to create complex polymeric colloidal morphologies, *Adv. Colloid Interface Sci.*, 2021, **294**, 102474.

27 T. Chen, Y. Peng, M. Qiu, C. Yi and Z. Xu, Recent advances in mixing-induced nanoprecipitation: from creating complex nanostructures to emerging applications beyond biomedicine, *Nanoscale*, 2023, **15**, 3594–3609.

28 G. Kim, J. Park, B. M. Kim, J. Kim, K.-J. Kim and J. Park, Influence of nanoprecipitation techniques on lignin nanoparticle structure, *Colloids Surf., A*, 2024, **682**, 132803.

29 D. Lohse and X. Zhang, Surface nanobubbles and nanodroplets, *Rev. Mod. Phys.*, 2015, **87**, 981.

30 Y. C. Wong, S. Yang and W. Wen, Prednisolone nanoprecipitation with Dean instability microfluidics mixer, *Nanomaterials*, 2024, **14**, 652.

31 C. B. Whitehead, S. Özkar and R. G. Finke, Lamer's 1950 model of particle formation: a review and critical analysis of its classical nucleation and fluctuation theory basis, of competing models and mechanisms for phase-changes and particle formation, and then of its application to silver halide, semiconductor, metal, and metal-oxide nanoparticles, *Mater. Adv.*, 2021, **2**, 186–235.

32 Q. Lei, F. He, X. Zhao and J. Yin, Preparation of poly(ionic liquid) microbeads by evaporation-assisted phase separation, *Macromol. Chem. Phys.*, 2022, **223**, 2100379.

33 E. Lepeltier, C. Bourgaux and P. Couvreur, Nanoprecipitation and the "Ouzo effect": Application to drug delivery devices, *Adv. Drug Delivery Rev.*, 2014, **71**, 86–97.

34 J. Meng, J. B. You, H. Hao, X. Tan and X. Zhang, Primary submicron particles from early stage asphaltene precipitation revealed in situ by total internal reflection fluorescence microscopy in a model oil system, *Fuel*, 2021, **296**, 120584.

35 J. Meng, C. Kanike, S. G. Sontti, A. Atta, X. Tan and X. Zhang, Asphaltene precipitation under controlled mixing conditions in a microchamber, *Chem. Eng. J.*, 2023, **451**, 138873.

36 J. Meng, S. G. Sontti and X. Zhang, Review of microscale dynamics of dilution-induced asphaltene precipitation under controlled mixing conditions, *Energy Fuels*, 2022, **36**, 13985–13999.

37 X. H. Zhang, A. Khan and W. A. Ducker, A nanoscale gas state, *Phys. Rev. Lett.*, 2007, **98**, 136101.

38 X. Zhang and D. Lohse, Perspectives on surface nanobubbles, *Biomicrofluidics*, 2014, **8**, 041301.

39 C. M. Hamadani, F. Mahdi, A. Merrell, J. Flanders, R. Cao, P. Vashisth, G. S. Dasanayake, D. S. Darlington, G. Singh and M. C. Pride, *et al.*, Ionic liquid coating-driven

nanoparticle delivery to the brain: Applications for Neuro-HIV, *Adv. Sci.*, 2024, **11**, 2305484.

40 H. Yu, B. P. Dyett, S. K. Pathirannahalage, M. Li, C. J. Drummond and T. L. Greaves, Formation of surface protic ionic liquid nanodroplets for nanofabrication, *Adv. Mater. Interfaces*, 2020, **7**, 1901647.

41 E. Lim, B. Kim, M. S. Oh and J. B. You, Microfluidic formation of surface nanodroplets using green deep eutectic solvents for liquid–liquid nanoextraction and controlled precipitation, *J. Colloid Interface Sci.*, 2023, **643**, 82–91.

42 S. V. Dalvi and R. N. Dave, Controlling particle size of a poorly water-soluble drug using ultrasound and stabilizers in antisolvent precipitation, *Ind. Eng. Chem. Res.*, 2009, **48**, 7581–7593.

43 N. T. Thanh, N. Maclean and S. Mahiddine, Mechanisms of nucleation and growth of nanoparticles in solution, *Chem. Rev.*, 2014, **114**, 7610–7630.

44 B. K. Wilson and R. K. Prud'homme, Co-encapsulation of organic polymers and inorganic superparamagnetic iron oxide colloidal crystals requires matched diffusion time scales, *Soft Matter*, 2024, **20**, 8312–8325.

45 G. Bovone, L. Cousin, F. Steiner and M. W. Tibbitt, Solvent controls nanoparticle size during nanoprecipitation by limiting block copolymer assembly, *Macromolecules*, 2022, **55**, 8040–8048.

46 S. L. Pal, U. Jana, P. K. Manna, G. P. Mohanta and R. Manavalan, Nanoparticle: An overview of preparation and characterization, *J. Appl. Pharm. Sci.*, 2011, 228–234.

47 S. Hornig, T. Heinze, C. R. Becer and U. S. Schubert, Synthetic polymeric nanoparticles by nanoprecipitation, *J. Mater. Chem.*, 2009, **19**, 3838–3840.

48 T. Pulingam, P. Foroozandeh, J.-A. Chuah and K. Sudesh, Exploring various techniques for the chemical and biological synthesis of polymeric nanoparticles, *Nanomaterials*, 2022, **12**, 576.

49 I. Perevyazko, A. Vollrath, S. Hornig, G. M. Pavlov and U. S. Schubert, Characterization of poly(methyl methacrylate) nanoparticles prepared by nanoprecipitation using analytical ultracentrifugation, dynamic light scattering, and scanning electron microscopy, *J. Polym. Sci., Part A: Polym. Chem.*, 2010, **48**, 3924–3931.

50 J. H. Lee, S. Y. Park, I.-G. Choi and J. W. Choi, Investigation of molecular size effect on the formation of lignin nanoparticles by nanoprecipitation, *Appl. Sci.*, 2020, **10**, 4910.

51 X. Wang, M. Wang, H. Zhao, J. Liu, M. Xing, H. Huang, M. A. C. Stuart and J. Wang, Flash nanoprecipitation enables regulated formulation of soybean protein isolate nanoparticles, *Food Hydrocolloids*, 2022, **131**, 107798.

52 H. S. Ali, P. York and N. Blagden, Preparation of hydrocortisone nanosuspension through a bottom-up nanoprecipitation technique using microfluidic reactors, *Int. J. Pharm.*, 2009, **375**, 107–113.

53 Y. Farrag, B. Montero, M. Rico, L. Barral and R. Bouza, Preparation and characterization of nano and micro particles of poly(3-hydroxybutyrate-*co*-3-hydroxyvalerate)(PHBV) via

emulsification/solvent evaporation and nanoprecipitation techniques, *J. Nanopart. Res.*, 2018, **20**, 1–17.

54 Y. He, X. Fan, J. Sun, R. Liu, Z. Fan, Z. Zhang, X. Chang, B. Wang, F. Gao and L. Wang, Flash nanoprecipitation of ultra-small semiconducting polymer dots with size tunability, *Chem. Commun.*, 2020, **56**, 2594–2597.

55 A. Manohar, M. G. Basavaraj, S. Sudhakar and E. Mani, Drying-induced flash nanoprecipitation in a sessile drop: A route to synthesize polymeric nanoparticles, *Langmuir*, 2024, **40**, 13613–13621.

56 E. Lamparelli, M. Marino, M. Scognamiglio, R. D'Auria, A. Santoro and G. Della Porta, PLA/PLGA nanocarriers fabricated by microfluidics-assisted nanoprecipitation and loaded with rhodamine or gold can be efficiently used to track their cellular uptake and distribution, *Int. J. Pharm.*, 2024, **667**, 124934.

57 J. Guo, W. Dai, W. Wu, S. Zhuang, H. Zhang and L. Cen, Microfluidic nanoprecipitation of PEGylated PLGA nanoparticles with rapamycin and performance evaluation, *J. Biomater. Sci., Polym. Ed.*, 2024, **35**, 1197–1213.

58 S. Gimondi, H. Ferreira, R. L. Reis and N. M. Neves, Microfluidic devices: a tool for nanoparticle synthesis and performance evaluation, *ACS Nano*, 2023, **17**, 14205–14228.

59 M. Abdelkarim, N. H. Abd Ellah, M. Elsabahy, M. Abdelgwad and S. A. Abouelmagd, Microchannel geometry vs flow parameters for controlling nanoprecipitation of polymeric nanoparticles, *Colloids Surf., A*, 2021, **611**, 125774.

60 J. Wang, W. Chen, J. Sun, C. Liu, Q. Yin, L. Zhang, Y. Xianyu, X. Shi, G. Hu and X. Jiang, A microfluidic tubing method and its application for controlled synthesis of polymeric nanoparticles, *Lab Chip*, 2014, **14**, 1673–1677.

61 M. Abdelkarim, N. H. Abd Ellah, M. Elsabahy, M. Abdelgwad and S. A. Abouelmagd, Microchannel geometry *vs.* flow parameters for controlling nanoprecipitation of polymeric nanoparticles, *Colloids Surf., A*, 2021, **611**, 125774.

62 R. A. Slater, T. O. McDonald, D. J. Adams, E. R. Draper, J. V. Weaver and S. P. Rannard, Architecture-driven aqueous stability of hydrophobic, branched polymer nanoparticles prepared by rapid nanoprecipitation, *Soft Matter*, 2012, **8**, 9816–9827.

63 X. Jia, Y. Yan, A. B. Kayitmazer, Y. Li and Y. Xu, Scalable yielding of highly stable polyelectrolyte-coated copper sulfide nanoparticles by flash nanoprecipitation for photothermal-chemotherapeutics, *Adv. Funct. Mater.*, 2021, **31**, 2100452.

64 Z. Zhu, P. Xu, G. Fan, N. Liu, S. Xu, X. Li, H. Xue, C. Shao and Y. Guo, Fast synthesis and separation of nanoparticles *via in situ* reactive flash nanoprecipitation and pH tuning, *Chem. Eng. J.*, 2019, **356**, 877–885.

65 M. Wang, N. Yang, Z. Guo, K. Gu, A. Shao, W. Zhu, Y. Xu, J. Wang, R. K. Prud'homme and X. Guo, Facile preparation of AIE-active fluorescent nanoparticles through flash nanoprecipitation, *Ind. Eng. Chem. Res.*, 2015, **54**, 4683–4688.

66 E. Ma, K. Chen, L. Sun, Z. Fu, J. Guo, J. Liu, J. Zhao, Z. Liu, Z. Lei and L. Li, *et al.*, Rapid construction of green

nanopesticide delivery systems using sophorolipids as surfactants by flash nanoprecipitation, *J. Agric. Food Chem.*, 2022, **70**, 4912–4920.

67 K. M. Pustulka, A. R. Wohl, H. S. Lee, A. R. Michel, J. Han, T. R. Hoye, A. V. McCormick, J. Panyam and C. W. Macosko, Flash nanoprecipitation: particle structure and stability, *Mol. Pharmaceutics*, 2013, **10**, 4367–4377.

68 W. Ye, G. Zhang, X. Liu, Q. Ren, F. Huang and Y. Yan, Fabrication of polysaccharide-stabilized zein nanoparticles by flash nanoprecipitation for doxorubicin sustained release, *J. Drug Delivery Sci. Technol.*, 2022, **70**, 103183.

69 Q.-W. Zhan and Y. Huang, Continuous and large-scale fabrication of lecithin stabilized nanoparticles with predictable size and stability using flash nano-precipitation, *LWT*, 2021, **139**, 110558.

70 R. Huang, C.-M. Hirschbiegel, X. Zhang, A. Gupta, S. Fedeli, Y. Xu and V. M. Rotello, Engineered polymer-supported biorthogonal nanocatalysts using flash nanoprecipitation, *ACS Appl. Mater. Interfaces*, 2022, **14**, 31594–31600.

71 H. Zhao, M. Wang, X. Wang, J. Liu, M. Xing, H. Huang, M. A. Cohen Stuart and J. Wang, Controlled fabrication of drug-loaded protein nanoparticles *via* flash nanoprecipitation, *AIChE J.*, 2023, **69**, e17941.

72 F. Bally, D. K. Garg, C. A. Serra, Y. Hoarau, N. Anton, C. Brochon, D. Parida, T. Vandamme and G. Hadziioannou, Improved size-tunable preparation of polymeric nanoparticles by microfluidic nanoprecipitation, *Polymer*, 2012, **53**, 5045–5051.

73 J. Bergfreund, S. Siegenthaler, V. Lutz-Bueno, P. Bertsch and P. Fischer, Surfactant adsorption to different fluid interfaces, *Langmuir*, 2021, **37**, 6722–6727.

74 T. Trantidou, Y. Elani, E. Parsons and O. Ces, Hydrophilic surface modification of PDMS for droplet microfluidics using a simple, quick, and robust method *via* PVA deposition, *Microsyst. Nanoeng.*, 2017, **3**, 1–9.

75 A. Gokaltun, M. L. Yarmush, A. Asatekin and O. B. Usta, Recent advances in nonbiofouling pdms surface modification strategies applicable to microfluidic technology, *Technology*, 2017, **5**, 1–12.

76 M. Gonçalves, I. M. Gonçalves, J. Borges, V. Faustino, D. Soares, F. Vaz, G. Minas, R. Lima and D. Pinho, Polydimethylsiloxane surface modification of microfluidic devices for blood plasma separation, *Polymers*, 2024, **16**, 1416.

77 F. Heshmatnezhad and A. R. S. Nazar, Synthesis of polycaprolactone nanoparticles through flow-focusing microfluidic-assisted nanoprecipitation, *Chem. Eng. Technol.*, 2020, **43**, 2073–2082.

78 E. Chiesa, R. Dorati, T. Modena, B. Conti and I. Genta, Multivariate analysis for the optimization of microfluidics-assisted nanoprecipitation method intended for the loading of small hydrophilic drugs into PLGA nanoparticles, *Int. J. Pharm.*, 2018, **536**, 165–177.

79 H. Chen, A. E. Celik, A. Mutschler, A. Combes, A. Runser, A. S. Klymchenko, S. Lecommandoux, C. A. Serra and

A. Reisch, Assembly of fluorescent polymer nanoparticles using different microfluidic mixers, *Langmuir*, 2022, **38**, 7945–7955.

80 T. Baby, Y. Liu, G. Yang, D. Chen and C.-X. Zhao, Microfluidic synthesis of curcumin loaded polymer nanoparticles with tunable drug loading and pH-triggered release, *J. Colloid Interface Sci.*, 2021, **594**, 474–484.

81 W. Li, Q. Chen, T. Baby, S. Jin, Y. Liu, G. Yang and C.-X. Zhao, Insight into drug encapsulation in polymeric nanoparticles using microfluidic nanoprecipitation, *Chem. Eng. Sci.*, 2021, **235**, 116468.

82 D. Liu, H. Zhang, S. Cito, J. Fan, E. Makila, J. Salonen, J. Hirvonen, T. M. Sikanen, D. A. Weitz and H. A. Santos, Core/shell nanocomposites produced by superfast sequential microfluidic nanoprecipitation, *Nano Lett.*, 2017, **17**, 606–614.

83 L. B. Neves, I. S. Afonso, G. Nobrega, L. G. Barbosa, R. A. Lima and J. E. Ribeiro, A review of methods to modify the PDMS surface wettability and their applications, *Micromachines*, 2024, **15**, 670.

84 G. Bovone, L. Cousin, F. Steiner and M. W. Tibbitt, Solvent controls nanoparticle size during nanoprecipitation by limiting block copolymer assembly, *Macromolecules*, 2022, **55**, 8040–8048.

85 Z. Fu, Y. Bao, Y. Zhang, Z. Yang, L. Zhou, L. Li, S. Dai, X. Hu and X. Guo, Precise structure-tailoring of multicomponent nanocatalysts enabled by continuous flow-controlled flash nanoprecipitation technique, *Sep. Purif. Technol.*, 2024, **351**, 128008.

86 W. D. Wong, M. F. Majnis, C. W. Lai, S. Sagadevan and N. M. Julkapli, Enhancement of mixing and reaction efficiency of various fluids applications at different microfluidic configuration and design, *Chem. Eng. Process.*, 2024, 109729.

87 H. Ma, M. Luo and L. L. Dai, Influences of surfactant and nanoparticle assembly on effective interfacial tensions, *Phys. Chem. Chem. Phys.*, 2008, **10**, 2207–2213.

88 K. H. Lee, G. Yang, B. E. Wyslouzil and J. O. Winter, Electrohydrodynamic mixing-mediated nanoprecipitation for polymer nanoparticle synthesis, *ACS Appl. Polym. Mater.*, 2019, **1**, 691–700.

89 K. H. Lee, F. N. Khan, I. B. Cosmin, D. U. Mualen, T. K. Porter, B. E. Wyslouzil and J. O. Winter, Semibatch and continuous electrohydrodynamic mixing nanoprecipitation for scalable polymer nanostructure production, *ACS Appl. Polym. Mater.*, 2024, **6**, 12382–12393.

90 H. Hadidi, E. Zandi, M. Al-Bahrani and R. Kamali, Fast electrokinetic mixing in microflows with different electrical conductivities, *Chem. Eng. Process.*, 2024, **199**, 109745.

91 A.-G. Niculescu, D. E. Mihaiescu and A. M. Grumezescu, A review of microfluidic experimental designs for nanoparticle synthesis, *Int. J. Mol. Sci.*, 2022, **23**, 8293.

92 A. Bendre, V. Hegde, K. V. Ajeya, S. Thagare Manjunatha, D. Somasekhara, V. K. Nadumane, K. Kant, H.-Y. Jung, W.-S. Hung and M. D. Kurkuri, Microfluidic-assisted synthesis of metal—organic framework—alginate micro-particles for sustained drug delivery, *Biosensors*, 2023, **13**, 737.

93 N. Rohra, G. Gaikwad, P. Dandekar and R. Jain, Microfluidic synthesis of a bioactive metal-organic framework for glucose-responsive insulin delivery, *ACS Appl. Mater. Interfaces*, 2022, **14**, 8251–8265.

94 E. Thomée, Microfluidic nanoparticle synthesis: a short review, *Elveflow*, 2021.

95 E. Piacentini, B. Russo, F. Bazzarelli and L. Giorno, Membrane nanoprecipitation: From basics to technology development, *J. Membr. Sci.*, 2022, 120564.

96 Z. Roshan, V. Haddadi-Asl, H. Ahmadi and M. Moussaei, Curcumin-encapsulated poly(lactic-*co*-glycolic acid) nanoparticles: A comparison of drug release kinetics from particles prepared *via* electrospray and nanoprecipitation, *Macromol. Mater. Eng.*, 2024, 2400040.

97 S. Zhao, C. Huang, X. Yue, X. Li, P. Zhou, A. Wu, C. Chen, Y. Qu and C. Zhang, Application advance of electrosprayed micro/nanoparticles based on natural or synthetic polymers for drug delivery system, *Mater. Des.*, 2022, 110850.

98 C. Mora-Huertas, H. Fessi and A. Elaissari, Influence of process and formulation parameters on the formation of submicron particles by solvent displacement and emulsification–diffusion methods: Critical comparison, *Adv. Colloid Interface Sci.*, 2011, **163**, 90–122.

99 M. Beck-Broichsitter, Solvent impact on polymer nanoparticles prepared nanoprecipitation, *Colloids Surf., A*, 2021, **625**, 126928.

100 K. C. Song, H. S. Lee, I. Y. Choung, K. I. Cho, Y. Ahn and E. J. Choi, The effect of type of organic phase solvents on the particle size of poly(D,L-lactide-*co*-glycolide) nanoparticles, *Colloids Surf., A*, 2006, **276**, 162–167.

101 X. Yan, J. Bernard and F. Ganachaud, Nanoprecipitation as a simple and straightforward process to create complex polymeric colloidal morphologies, *Adv. Colloid Interface Sci.*, 2021, **294**, 102474.

102 Y. Herdiana, N. Wathoni, S. Shamsuddin and M. Muchtaridi, Scale-up polymeric-based nanoparticles drug delivery systems: Development and challenges, *OpenNano*, 2022, **7**, 100048.

103 J. Tao, S. F. Chow and Y. Zheng, Application of flash nanoprecipitation to fabricate poorly water-soluble drug nanoparticles, *Acta Pharm. Sin. B*, 2019, **9**, 4–18.

104 A. Bendre, M. P. Bhat, K.-H. Lee, T. Altalhi, M. A. Alruqi and M. Kurkuri, Recent developments in microfluidic technology for synthesis and toxicity-efficiency studies of biomedical nanomaterials, *Mater. Today Adv.*, 2022, **13**, 100205.

105 W. Huang and C. Zhang, Tuning the size of poly(lactic-*co*-glycolic acid)(PLGA) nanoparticles fabricated by nanoprecipitation, *Biotechnol. J.*, 2018, **13**, 1700203.

106 A. Bukhari, A. Idris and M. Atta, Effect of organic and aqueous dispersion medium on the development of polystyrene nanoparticles in nanoprecipitation method, *Malays. J. Fundam. Appl. Sci.*, 2014, **10**, 28–32.

107 S. Hornig and T. Heinze, Efficient approach to design stable water-dispersible nanoparticles of hydrophobic cellulose esters, *Biomacromolecules*, 2008, **9**, 1487–1492.

108 H. Shen, S. Hong, R. K. Prud'homme and Y. Liu, Self-assembling process of flash nanoprecipitation in a multi-inlet vortex mixer to produce drug-loaded polymeric nano-particles, *J. Nanopart. Res.*, 2011, **13**, 4109–4120.

109 L. S. Grundy, V. E. Lee, N. Li, C. Sosa, W. D. Mulhearn, R. Liu, R. A. Register, A. Nikoubashman, R. K. Prud'homme, A. Z. Panagiotopoulos and R. D. Priestley, Rapid production of internally structured colloids by flash nanoprecipitation of block copolymer blends, *ACS Nano*, 2018, **12**, 4660–4668, PMID: 29723470.

110 L. Capretto, W. Cheng, D. Carugo, O. L. Katsamenis, M. Hill and X. Zhang, Mechanism of co-nanoprecipitation of organic actives and block copolymers in a microfluidic environment, *Nanotechnology*, 2012, **23**, 375602.

111 Q. Feng, L. Zhang, C. Liu, X. Li, G. Hu, J. Sun and X. Jiang, Microfluidic based high throughput synthesis of lipid-polymer hybrid nanoparticles with tunable diameters, *Biomicrofluidics*, 2015, **9**, 052604.

112 E. Aschenbrenner, K. Bley, K. Koynov, M. Makowski, M. Kappl, K. Landfester and C. K. Weiss, Using the poly-meric ouzo effect for the preparation of polysaccharide-based nanoparticles, *Langmuir*, 2013, **29**, 8845–8855.

113 J. P. Rao and K. E. Geckeler, Polymer nanoparticles: Preparation techniques and size-control parameters, *Prog. Polym. Sci.*, 2011, **36**, 887–913.

114 P. Dwivedi, K. M. Karumbaiah and R. Das, Nano-size poly-mers *via* precipitation of polymer solutions, *Nano-size poly-mers: preparation, properties, applications*, 2016, pp. 251–282.

115 J. Aubry, F. Ganachaud, J.-P. Cohen Addad and B. Cabane, Nanoprecipitation of polymethylmethacrylate by solvent shifting: 1. boundaries, *Langmuir*, 2009, **25**, 1970–1979.

116 R. Donno, A. Gennari, E. Lallana, J. M. R. De La Rosa, R. d'Arcy, K. Treacher, K. Hill, M. Ashford and N. Tirelli, Nanomanufacturing through microfluidic-assisted nano-precipitation: Advanced analytics and structure-activity relationships, *Int. J. Pharm.*, 2017, **534**, 97–107.

117 A. G. Luque-Alcaraz, J. Lizardi-Mendoza, F. Goycoolea, I. Higuera-Ciapara and W. Argüelles-Monal, Preparation of chitosan nanoparticles by nanoprecipitation and their ability as a drug nanocarrier, *RSC Adv.*, 2016, **6**, 59250–59256.

118 V. I. Vorobyova, Plant extract based on deep eutectic solvent-mediated biosynthesis of silver nanoparticles: Cytotoxicity and antibacterial effects, *Bioinorg. Chem. Appl.*, 2023, **2023**, 9672432.

119 Z. Tshemese, S. C. Masikane, S. Mlowe and N. Reva-prasadu, Progress in green solvents for the stabilisation of nanomaterials: imidazolium based ionic liquids, *Recent Advances in Ionic Liquids*, 2018, vol. 69.

120 D. A. Patino-Ruiz, S. I. Meramo-Hurtado, A. D. González-Delgado and A. Herrera, Environmental sustainability evalua-tion of iron oxide nanoparticles synthesized via green synth-esis and the coprecipitation method: A comparative life cycle assessment study, *ACS Omega*, 2021, **6**, 12410–12423.

121 N. Kučuk, M. Primožič, Ž. Knez and M. Leitgeb, Sustain-able biodegradable biopolymer-based nanoparticles for healthcare applications, *Int. J. Mol. Sci.*, 2023, **24**, 3188.

122 F. Tivano and V. Chiono, Zein as a renewable material for the preparation of green nanoparticles for drug delivery, *Front. Biomater. Sci.*, 2023, **2**, 1156403.

123 A. Goyanes, A. B. Buanz, A. W. Basit and S. Gaisford, Fused-filament 3D printing (3DP) for fabrication of tablets, *Int. J. Pharm.*, 2014, **476**, 88–92.

124 M. J. Garland, E. Caffarel-Salvador, K. Migalska, A. D. Woolfson and R. F. Donnelly, Dissolving polymeric micro-needle arrays for electrically assisted transdermal drug delivery, *J. Controlled Release*, 2012, **159**, 52–59.

125 Z. Ping, X. Hu, L. Wang, J. Shi, Y. Tao, X. Wu, Z. Hou, X. Guo, W. Zhang and H. Yang, *et al.*, Melatonin attenuates titanium particle-induced osteolysis *via* activation of Wnt/β-catenin signaling pathway, *Acta Biomater.*, 2017, **51**, 513–525.

126 J. Bidone, R. S. Schuh, M. Farinon, É. Poletto, G. Pasqualim, P. G. de Oliveira, M. Fraga, R. M. Xavier, G. Baldo and H. F. Teixeira, *et al.*, Intra-articular nonviral gene therapy in mucopolysaccharidosis I mice, *Int. J. Pharm.*, 2018, **548**, 151–158.

127 C. Tao, T. Huo, M. Zhang, Z. Chen, X. Zhang and H. Song, Evaluation of the stability and absorption of tacrolimus self-microemulsifying drug delivery system, *J. Drug Delivery Sci. Technol.*, 2020, **57**, 101640.

128 G. Yang, Y. Liu, S. Jin, Y. Hui, X. Wang, L. Xu, D. Chen, D. Weitz and C.-X. Zhao, Phase separation-induced nano-precipitation for making polymer nanoparticles with high drug loading, *Aggregate*, 2023, e314.

129 Y. Liu, G. Yang, T. Baby, D. Chen, D. A. Weitz and C.-X. Zhao, Stable polymer nanoparticles with exceptionally high drug loading by sequential nanoprecipitation, *Angew. Chem.*, 2020, **132**, 4750–4758.

130 K. A. K. Azman, F. C. Seong, G. K. S. Singh and M. M. R. M. M. Affandi, Physicochemical characterization of astaxan-thin-loaded PLGA formulation *via* nanoprecipitation tech-nique, *J. Appl. Pharm. Sci.*, 2021, **11**, 056–061.

131 S. Chopra, N. Bertrand, J.-M. Lim, A. Wang, O. C. Farokhzad and R. Karnik, Design of insulin-loaded nano-particles enabled by multistep control of nanoprecipita-tion and zinc chelation, *ACS Appl. Mater. Interfaces*, 2017, **9**, 11440–11450.

132 M. Haim Zada, Y. Rottenberg and A. J. Domb, Peptide loaded polymeric nanoparticles by non-aqueous nanopre-cipitation, *J. Colloid Interface Sci.*, 2022, **622**, 904–913.

133 H. D. Lu, K. D. Ristroph, E. L. K. Dobrijevic, J. Feng, S. A. McManus, Y. Zhang, W. D. Mulhearn, H. Ramachandruni, A. Patel and R. K. Prud'homme, Encapsulation of OZ439 into nanoparticles for supersaturated drug release in oral malaria therapy, *ACS Infect. Dis.*, 2018, **4**, 970–979, PMID: 29575888.

134 Z. Qi, Y. Qiu, Z. Zhong, J. Wang, W. Bian, M. A. C. Stuart and M. Wang, Regulated preparation of celastrol-loaded nanoparticle by flash nanoprecipitation, *J. Drug Delivery Sci. Technol.*, 2022, **69**, 103146.

135 N. J. Caggiano, B. K. Wilson, R. D. Priestley and R. K. Prud'homme, Development of an *in vitro* release

assay for low-density cannabidiol nanoparticles prepared by flash nanoprecipitation, *Mol. Pharmaceutics*, 2022, **19**, 1515–1525.

136 Z. Zeng, P. Zhao, L. Liu, X. Gao, H.-Q. Mao and Y. Chen, Lipid stabilized solid drug nanoparticles for targeted chemotherapy, *ACS Appl. Mater. Interfaces*, 2018, **10**, 24969–24974.

137 W. Ye, F. Zhu, Y. Cai, L. Wang, G. Zhang, G. Zhao, X. Chu, Q. Shuai and Y. Yan, Improved paclitaxel delivery with PEG-*b*-PLA/zein nanoparticles prepared *via* flash nanoprecipitation, *Int. J. Biol. Macromol.*, 2022, **221**, 486–495.

138 G. Song, M. Chen, Y. Zhang, L. Cui, H. Qu, X. Zheng, M. Wintermark, Z. Liu and J. Rao, Janus iron oxides@semiconducting polymer nanoparticle tracer for cell tracking by magnetic particle imaging, *Nano Lett.*, 2018, **18**, 182–189.

139 C. Yin, G. Wen, C. Liu, B. Yang, S. Lin, J. Huang, P. Zhao, S. H. D. Wong, K. Zhang and X. Chen, *et al.*, Organic semiconducting polymer nanoparticles for photoacoustic labeling and tracking of stem cells in the second near-infrared window, *ACS Nano*, 2018, **12**, 12201–12211.

140 J. Wang, M. Kuang, H. Duan, D. Chen and M. Jiang, pH-dependent multiple morphologies of novel aggregates of carboxyl-terminated polymide in water, *Eur. Phys. J. E: Soft Matter Biol. Phys.*, 2004, **15**, 211–215.

141 T. Higuchi, K. Motoyoshi, H. Sugimori, H. Jinnai, H. Yabu and M. Shimomura, Phase transition and phase transformation in block copolymer nanoparticles, *Macromol. Rapid Commun.*, 2010, **31**, 1773–1778.

142 Y. Yao, J. Li, X. Guo, J. Song, Z. Chang, J. Zeng, Y. Liu, J. Li, B. Dai and F. Yu, Up-scaled synthesis of flower-like SiO2 microspheres via continuous flash nanoprecipitation and their application as a catalyst support, *Energy Rep.*, 2020, **6**, 2724–2734.

143 H. Xie, Z.-G. She, S. Wang, G. Sharma and J. W. Smith, One-step fabrication of polymeric Janus nanoparticles for drug delivery, *Langmuir*, 2012, **28**, 4459–4463.

144 V. M. Jiménez-Pérez and K. Prakash, *et al.*, Thermal decomposition synthesis of cylindrical rod-like MoO3 and irregular sphere-like Ag2MoO4 nanocrystals for accelerating photocatalytic degradation of industrial reactive dyes and biosensing application, *J. Environ. Chem. Eng.*, 2023, **11**, 109371.

145 Y. Shi, Z. Lyu, M. Zhao, R. Chen, Q. N. Nguyen and Y. Xia, Noble-metal nanocrystals with controlled shapes for catalytic and electrocatalytic applications, *Chem. Rev.*, 2020, **121**, 649–735.

146 E. Middha, C. Chen, P. N. Manghnani, S. Wang, S. Zhen, Z. Zhao and B. Liu, Synthesis of uniform polymer encapsulated organic nanocrystals through Ouzo nanocrystallization, *Small Methods*, 2022, **6**, 2100808.

147 R. Xu, D. Dang, Z. Wang, Y. Zhou, Y. Xu, Y. Zhao, X. Wang, Z. Yang and L. Meng, Facilely prepared aggregation-induced emission (AIE) nanocrystals with deep-red emission for super-resolution imaging, *Chem. Sci.*, 2022, **13**, 1270–1280.

148 S. Thakkar and M. Misra, Electrospray drying of docetaxel nanosuspension: A study on particle formation and evaluation of nanocrystals thereof, *J. Drug Delivery Sci. Technol.*, 2020, **60**, 102009.

149 D. Cui, C. Xie and K. Pu, Development of semiconducting polymer nanoparticles for photoacoustic imaging, *Macromol. Rapid Commun.*, 2017, **38**, 1700125.

150 K. Pu, J. Mei, J. V. Jokerst, G. Hong, A. L. Antaris, N. Chattopadhyay, A. J. Shuhendler, T. Kurosawa, Y. Zhou and S. S. Gambhir, *et al.*, Diketopyrrolopyrrole-based semiconducting polymer nanoparticles for *in vivo* photoacoustic imaging, *Adv. Mater.*, 2015, **27**, 5184–5190.

151 A. Shanavas, N. K. Jain, N. Kaur, D. Thummuri, M. Prasanna, R. Prasad, V. G. M. Naidu, D. Bahadur and R. Srivastava, Polymeric core–shell combinatorial nanomedicine for synergistic anticancer therapy, *ACS Omega*, 2019, **4**, 19614–19622.